American Journal of Biomedical Sciences
ISSN: 1937-9080
nwpii.com/ajbms

Running Title: ANALYTICAL DERIVATION OF GAMMA PUTTY PARAMETERS

Analytical Derivation and Validation of Dosimetric Parameters for Gamma Putty Attenuators with Megavoltage Photon Beams

Aime M Gloi

Radiation Oncology - HSHS St Vincent Hospital, Wisconsin, USA
***Corresponding Author**
Aime M Gloi
Radiation Oncology
HSHS St Vincent Hospital
835 South Van Buren Street
Green Bay, WI 54301
USA
Email: agloi@sbcglobal.net

Received: 27 January 2017; | Revised: 18 July 2017; | Accepted: 29 August 2017

Abstract

Background: Several descriptors are used to characterize the dosimetric parameters of a photon beam through an attenuator. This study evaluates these descriptors analytically through various thicknesses of Gamma Putty. Specifically, we measure percent ionization depth doses as a function of depth and field size, and fit three models to the data. *Materials and Methods:* Measurements of percent ionization at various depths along the central axis were generated from 6 MV and 18 MV photon beams at a source-axis distance of 100 cm with an ionization in solid water phantom. We fit analytic models to the data to determine linear attenuation, beam hardening, beam quality, and electron contamination. *Results:* We report best-fit parameters for all the analytical models. All models yielded a root mean square (RMS) error of less than 1% with respect to the data. At depths below 5cm in the phantom, the largest attenuation coefficients (μ) were observed for the 6 MV beam, regardless of Gamma Putty thickness. Also, the smallest field sizes (4×4 and 5×5 cm^2) have the largest attenuation coefficients at these depths, for both beam energies. At a depth of 10 cm, the variation in μ was negligible for both beam energies. *Conclusions:* By fitting parametric models to axial ionization profiles, it is possible to characterize the dosimetric parameters of any attenuator as a function of thickness and field size, without knowing the precise spectral distribution of the beam. Parameters such as attenuation coefficients, beam hardening, and electron contamination can then be calculated accurately for any combination of field size and attenuator thickness.

Keywords: Analytic, beam hardening, electron contamination, Gamma Putty, beam quality index

1. Introduction

The aim of radiotherapy cancer treatment is to deliver a large dose to the tumor while minimizing its effect on the surrounding tissues. Some radiation therapies use compensators for missing tissue, in order to obtain a uniform dose distribution at the desired depth. In most cases, this is done either through a combination of beams, or by shaping the field using blocks made of different materials or multi-leaf collimators. The use of such modifiers influences the received radiation dose, quantified at certain reference points in a patient or phantom [1-2], and is subject to factors that include primary and scattered radiation [3-4]. These factors in turn are dependent on the atomic number of the material, beam energy, reference depth, and field size.

The literature contains several attempts to characterize the dosimetric parameters of radiotherapy modifiers, such as linear attenuation and beam hardening. The iterative method [5-8] has been used to determine linear attenuation coefficients for radiotherapy modifiers under a variety of conditions: depth, field size, components, and thickness. The linear attenuation coefficient, which can vary with depth through the tissue or phantom, is the result of several independent interaction processes between photons and atoms. For example, it includes photoelectric absorption, scattering, and pair production. By studying the attenuation of incident photon beams in a material, it is possible to identify its internal structure and composition. Furthermore, even through a simple analysis of the percent ionization depth dose (PDD) in an absorbing medium, it is possible to accurately model the beam's interaction with the patient. This procedure entails some prior experimental measurements to fit and validate a parametric model.

There are many advantages to this approach. First, it is easy to detect and explain outliers in the experimental data and also among the results published by different studies. Second, interpolation and correlation can be used to incorporate data published by other sources into the model, thereby reducing the number of measurements that needs to be collected on site. LeBron *et al*. [9] echo this assertion by advocating the portability of data sets and the ease of evaluating the characteristics of different materials. For instance, Du Plessis *et al*. [7] present a detailed analysis of linear attenuation measurements in several materials with different atomic numbers. Specifically, they use a Monte Carlo model with the DOSXYZ code to quantify the dependence of linear attenuation on field size for narrow beams. They also discuss the importance of lateral equilibrium in narrow beam geometries.

In related work, Bjärngard *et al*. [10] analyzed attenuation factors in high-energy x-ray beams, and provided a framework to determine the beam hardening and softening coefficients. Similarly, Kleinschmidt *et al*. [11] defined a beam hardening coefficient based on the change in the mean attenuation coefficient, and offered a formal definition of the average attenuation coefficient, $\langle\mu\rangle$. Alles *et al*. [12] discussed the theoretical basis of the average attenuation coefficient, explaining its behavior as a consequence of beam hardening and spectral width. El-Khatib *et al.* [1] published attenuation coefficients derived from lead modifiers, for several types of photon beams at various depths. They used an analytical expression based on Klein–Nishina coefficients and Compton scattering to calculate the first-order scatter induced by the lead modifier.

The objective of this study is twofold: to characterize the properties of Gamma Putty as a radiotherapy modifier, and to validate several functional representations of attenuation properties proposed in the literature. We used a megavoltage photon beam and examined the effects of field size, beam energy, and attenuator thickness on several dosimetric parameters and beam quality measures. First of these is the linear attenuation coefficient, as discussed above. Second, we evaluated D_{20}/D_{10}, a quality measure closely related to the mean attenuation coefficient of the photon beam. Third, when a photon beam strikes the attenuator, its spectrum can harden or soften, increasing or decreasing the mean photon energy respectively. Hence, we use the 10cm and 20cm depth doses to fit an analytical model that includes a beam hardening coefficient as one of its free parameters. Finally, we use the percent ionization dose curve to fit a model of electron contamination at the phantom surface.

2. Materials and methods

2.1 Measurements

To evaluate linear attenuation and the effects of beam hardening and softening, we measure relative ionization at various depths. Compensator blocks (attenuators) were manufactured from Gamma Putty (Shieldwerx, Rio Rancho, New Mexico, USA), which is iron poly putty (LDPE) loaded with 90% bismuth. Circular blocks of Gamma Putty (Fig. 1a) with various thicknesses (t=0.3, 0.5, 1.0, 1.5, 2.0, 2.5 cm) were positioned directly on solid water (CNMC, Nashville, USA) phantoms for the measurements. Ionization measurements were made along the central axis using a Farmer chamber (PTW FREIBURG, Freiburg, Germany), from a depth of 23 cm to the surface (Fig. 1b).

Megavoltage (6 and 18 MV) x-ray beams generated by a Varian 21 EX linear accelerator (Varian Medical systems Palo alto USA) were used for this study. Ionization data were recorded using an electrometer (Victoreen 500, Fluke Biomedical Radiation, Ohio, USA) at various depths in the solid water, both with and without a Gamma Putty modifier in place. The beams were shaped into square fields of various sizes (4×4cm^2, 5×5 cm^2, 6×6 cm^2, 7×7 cm^2, 8×8 cm^2, 9×9 cm^2, and 10×10 cm^2). The source-axis distance (SSD) was always 100 cm. In addition to full relative ionization depth profiles, we directly calculated the quality index D_{20}/D_{10} (the ratio of charge measured in the solid water at 20 cm and 10 cm depths).

Figure 1a. Circular blocks of Gamma Putty wrapped in plastic.

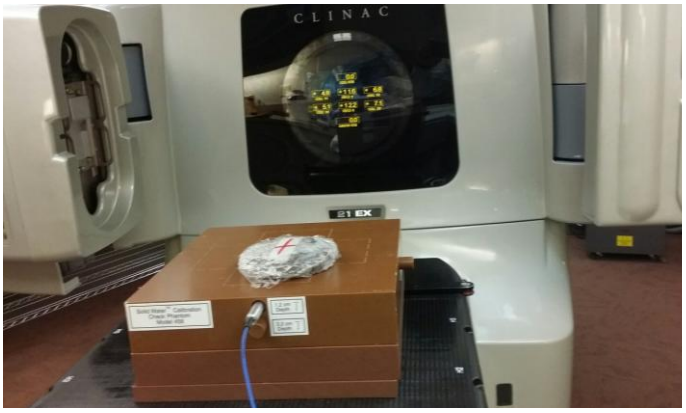

Figure 1b. Experimental setup for percent ionization depth dose measurements. The Gamma Putty block is lying on a solid water phantom under a Varian Linac 21 EX.

2.2 Analytical models

2.2.1 Attenuation coefficient

The attenuation factor for a given beam modifier is often assumed to be independent of field size, depth, and SSD. In fact, the attenuation factor not only depends on all these factors but also should be measured at depths well beyond the maximum range of electron contamination. A beam modifier in contact with the patient's skin has two effects on the dose profile. It attenuates the incident beam, as intended, but it also generates scattered radiation which enhances the primary beam inside the patient. The width of the incident beam in particular can have a significant effect on the profile of this scattered radiation. For this reason, several analytical models for the percentage ionization depth doses of a high-energy photon beam have been proposed in the literature. In this research, we fit several such models to our data and report the model parameters and attenuation factors inferred from the models.

The first model was proposed by Birgani *et al* [5]. For each attenuator thickness (t), the observed transmission curve is modeled as a function of field size (f). The transmission is modeled as a difference between two exponential curves, with a total of four free parameters, according to the following expression:

$$PDD(z, f) = \alpha(f)e^{-\beta(f)z} - \varsigma(f)e^{-\tau(f)z} \quad (1)$$

where *PDD* stands for the percentage ionization depth dose along the beam axis and *z* is the depth of the measurement inside the solid water phantom. The linear attenuation coefficient μ in this model is a function of depth and field size, given by:

$$\mu(z, f) = \frac{\alpha(f)\beta(f)e^{-\beta(f)z} - \tau(f)\varsigma(f)e^{-\tau(f)z}}{\alpha(f)e^{-\beta(f)z} - \varsigma(f)e^{-\tau(f)z}} \quad (2)$$

In the present work, the free parameters α, β, ς, τ were determined by least squares minimization, iteratively choosing them to obtain the best fit between the measured depth doses and the values obtained from equation (1). This was done using the Microsoft Excel ''solver'' function. The fitted values agree well with the data, with an average $R^2 \geq 0.998$. Note that *PDD* (*z, f*) includes the percentage ionization depth dose from both transmitted and scattered x-rays in the solid water phantom. The attenuation coefficients μ (*z, f*) obtained from this first model play a major role in characterizing the effects and utility of Gamma Putty as a beam modifier.

2.2.2 Beam hardening coefficient

The underlying complexity of beam modifiers and how they affect a megavoltage photon beam was also analyzed by Bjärngard *et al.* [10]. Our second model for percent depth ionization is based on their research:

$$PDD\,(d) = e^{-\acute{\upsilon} d\,(1\,-\,\eta d)} \quad (3)$$

where ύ and η are the attenuation factor and beam hardening coefficients respectively. This parameterization of PDD was performed using only two depth measurements (10 and 20 cm). Note that in addition to the expected hardening of the primary photon spectrum due to absorption of low-energy photons, the beam can also be softened by the continuous production of low-energy scattered photons, as described by Leung *et al* [13].

2.2.3 Beam quality

The overall beam quality was evaluated as D_{20}/D_{10}, the ratio of the percentage ionization doses measured at 20 cm and 10 cm in a parallel beam. These are the same measurements used to fit the beam hardening model of Eq. (3).

2.2.4 Electron contamination

Brahme *et al.* [14] provided an analytic model for the shape of the depth dose curve with three independent parameters:

$$PDD(z) = K(e^{-Az} - \nu e^{-Bz}) \quad (4)$$

Using this model, the bremsstrahlung dose at the surface is given by *K* (1.0−*v*). Brahme *et al*. [19] showed that the proportion of this does due to contaminating electrons is given by the expression (1.0−*v*). This model fits the full percent ionization depth dose curves with an RMS error smaller than 1% and a correlation coefficient $R^2 \geq 0.99$.

3. Results

3.1 Attenuation factor models

Figures 2-4 fit the results of our percent ionization curve measurements to the Birgani *et al*. [5] model. The curves labeled "calc" in the graphs are based on Eq. (1) and (2). These graphs show that the percent ionization depth curves are exponential for all field sizes and measurement depths. Compared to the 18 MV beam, the 6 MV beam exhibits a less prominent shoulder at d_{max}. Furthermore, the 18 MV beam is more penetrating than the 6 MV beam. This is true even with a Gamma Putty attenuator (Figures 3a and b), partly because of input from scattered photons. A large field size also raises the dose curve for all experiments, again due to the contribution of scattered photons. The average absolute error agreement between the data and the fitted models is ± 0.2% over a depth range of 0 to 23 cm, for all the experiments in Figures 2– 4. Tables 1 and 2 list some of the relevant parameters obtained by fitting the percent ionization depth dose to Eq. (1).

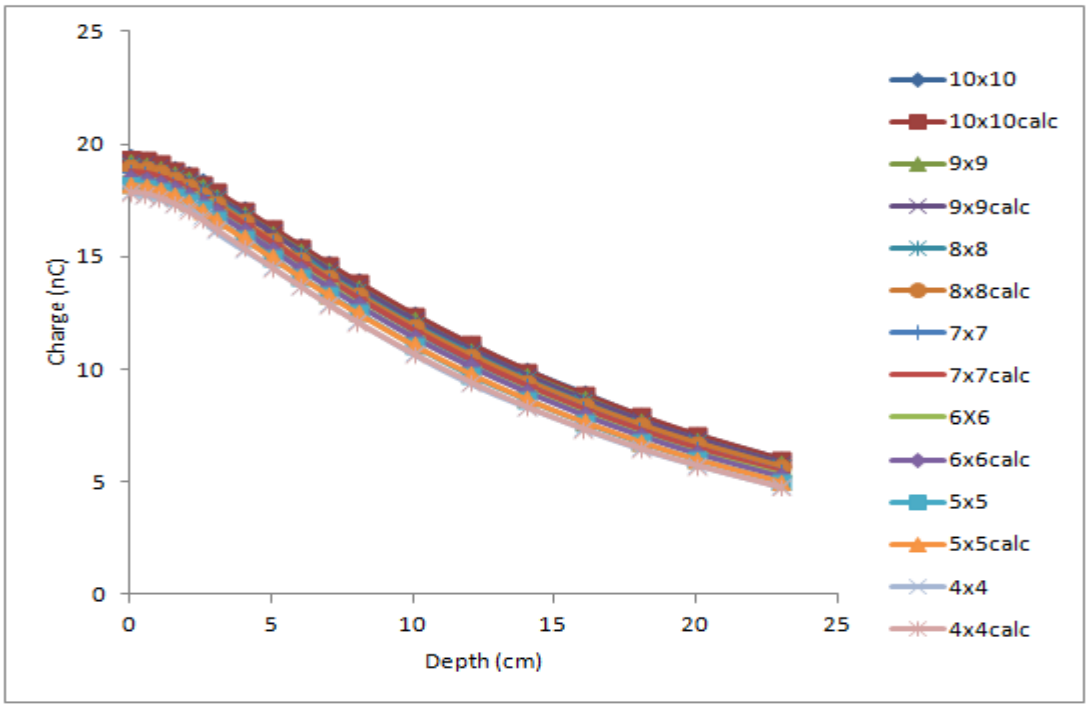

Figure 2a. Raw ionization data for the 6 MV beam and no Gamma Putty attenuator. The series labeled 'calc' are parametric fits to the data using Eq. (1).

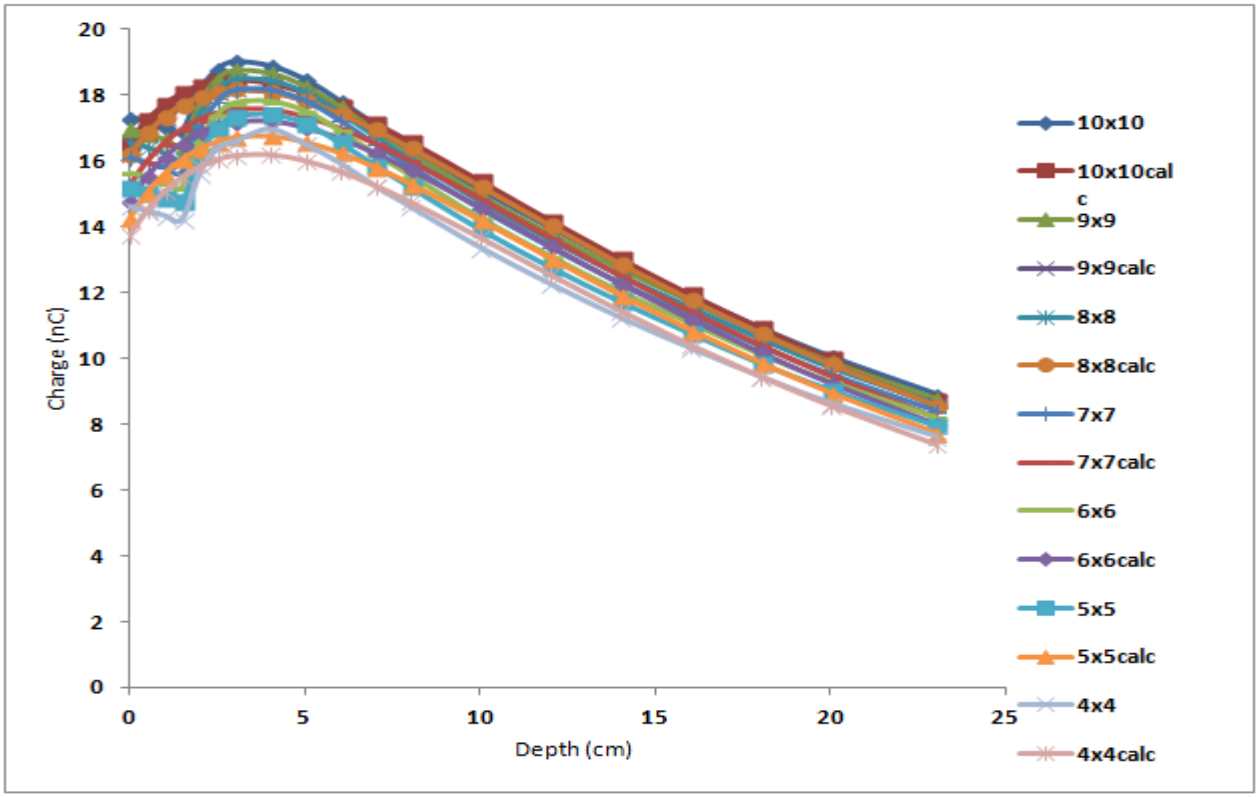

Figure 2b. Raw ionization data for the 18 MV beam and no Gamma Putty attenuator. The series labeled 'calc' are parametric fits to the data using Eq. (1).

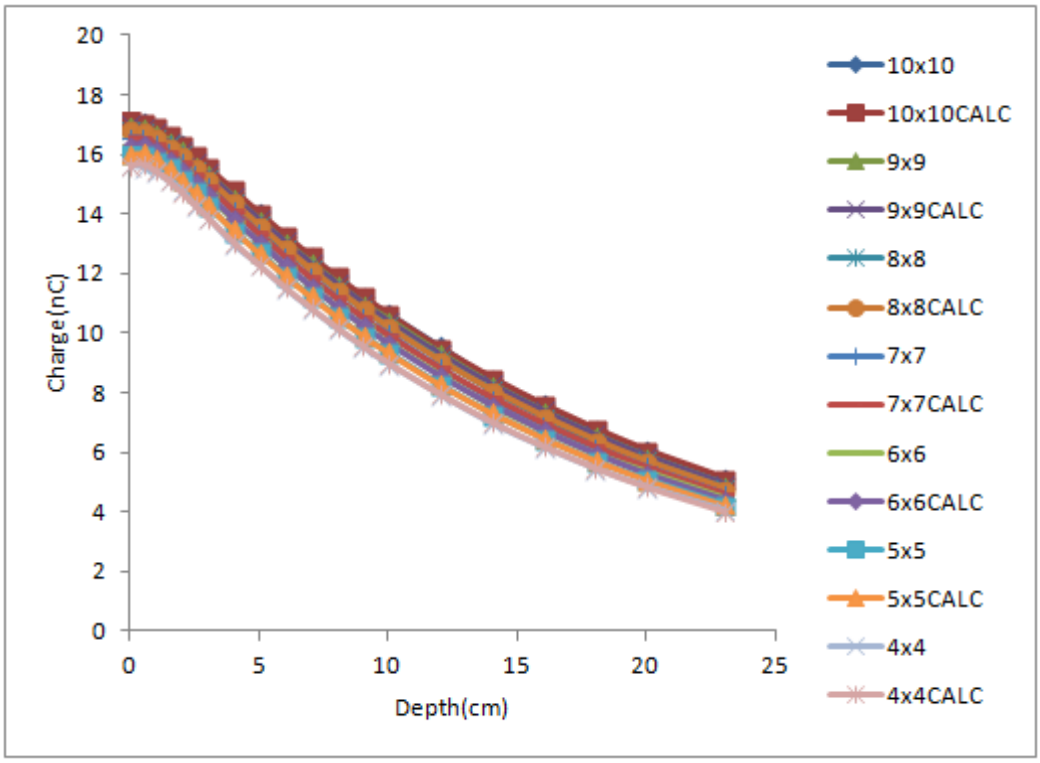

Figure 3a. Raw ionization data for the 6 MV beam and a Gamma Putty attenuator 0.5 cm thick. The series labeled 'calc' are parametric fits to the data using Eq. (1).

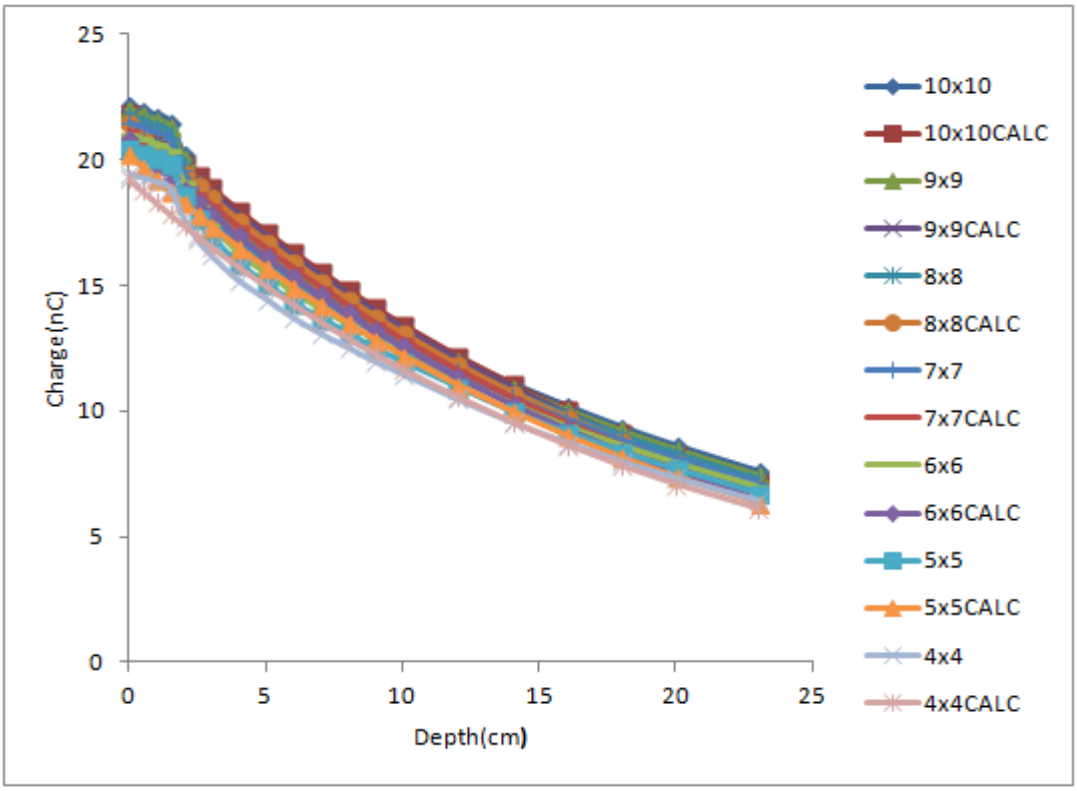

Figure 3b. Raw ionization data for the 18 MV beam and a Gamma Putty attenuator 0.5 cm thick. The series labeled 'calc' are parametric fits to the data using Eq. (1).

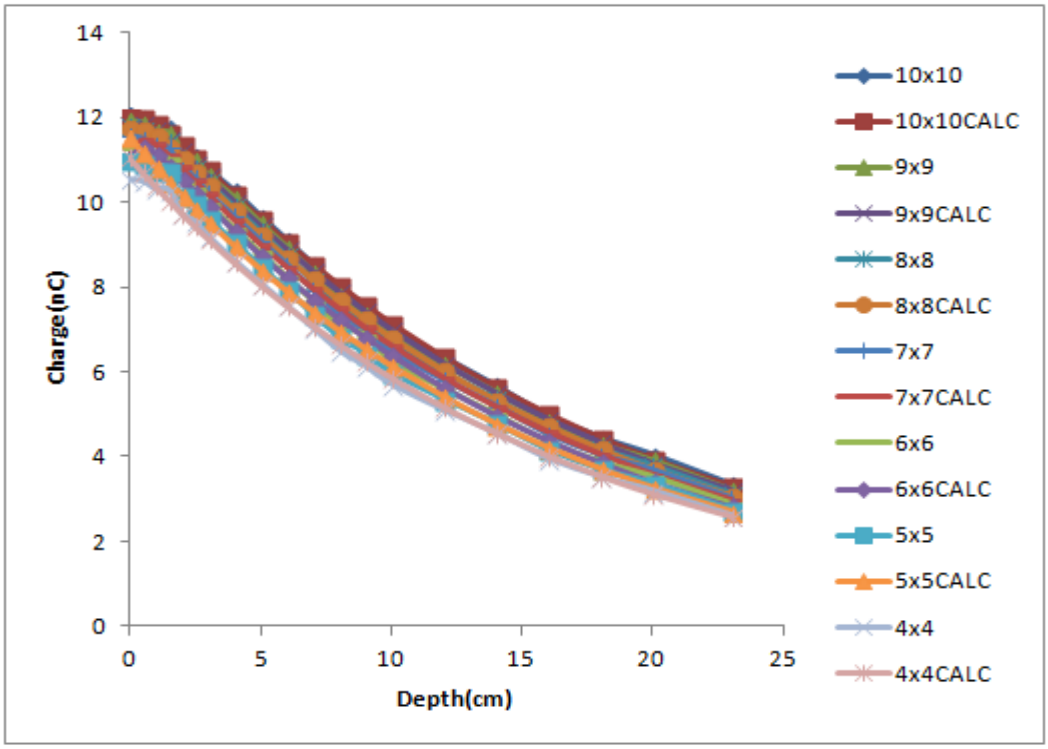

Figure 4a. Raw ionization data for the 6 MV beam and a Gamma Putty attenuator 2.5 cm thick. The series labeled 'calc' are parametric fits to the data using Eq. (1).

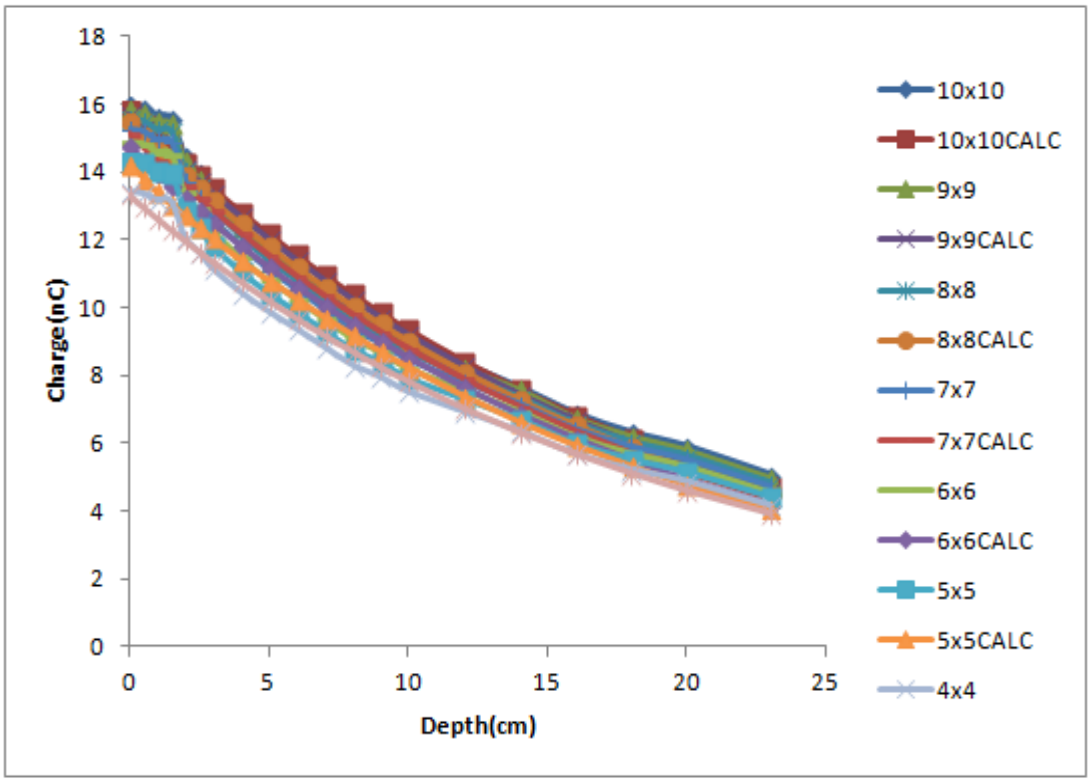

Figure 4b. Raw ionization data for the 18 MV beam and a Gamma Putty attenuator 2.5 cm thick. The series labeled 'calc' are parametric fits to the data using Eq. (1).

Table 1. Model parameters α (f), β (f), ς (f), ζ (f) for the 6 MV beam, for all combinations of field size and Gamma Putty thickness. All the parameters were calculated simultaneously by iterative methods.

Thickness (cm)	Parameters	Field sizes (cm^2)						
0		10x10	9x9	8x8	7x7	6x6	5x5	4x4
	α (f)	21.9044	21.6638	21.0890	21.2879	20.9210	20.5356	19.9863
	β (f)	0.0562	0.0569	0.0568	0.0592	0.0600	0.0613	0.0622
	ς (f)	2.5029	2.4609	2.0680	2.5309	2.4348	2.3479	2.1448
	ζ (f)	0.4884	0.5179	0.6040	0.5227	0.5590	0.5992	0.6487
0.3	α (f)	20.1805	19.0755	19.7142	19.4270	19.0838	18.6664	18.0072
	β (f)	0.0566	0.0538	0.0583	0.0592	0.0601	0.06105	0.0614
	ς (f)	1.9064	1.9064	1.7783	1.6941	1.5997	1.4936	1.1778
	ζ (f)	0.5931	0.5931	0.6752	0.6994	0.7682	0.8731	0.9409
0.5	α (f)	18.6253	18.4766	18.2601	17.9846	17.6523	17.2498	16.7517
	β (f)	0.0560	0.0571	0.0581	0.0591	0.0601	0.0611	0.0619
	ς (f)	1.4687	1.4692	1.4384	1.4082	1.3364	1.2465	1.1512
	ζ (f)	0.7122	0.7128	0.7658	0.9039	1.0283	1.1765	1.3683
1.0	α (f)	17.6266	17.4540	17.1690	16.8948	16.5230	16.0657	15.5666
	β (f)	0.0569	0.0578	0.0586	0.0595	0.0603	0.0610	0.0618
	ς (f)	1.6777	1.5871	1.5169	1.5301	1.5074	1.2433	1.3455
	ζ (f)	0.6086	0.6116	0.7225	0.7889	0.9710	1.0090	1.3492
1.5	α (f)	16.2616	16.1085	15.8814	15.6085	15.2728	14.8824	14.3681
	β (f)	0.0570	0.0580	0.0588	0.0597	0.0606	0.0614	0.0621
	ς (f)	0.9975	1.0331	0.9743	0.9863	1.1247	1.3371	2.5288
	ζ (f)	0.9675	1.0424	1.14036	1.3953	1.9226	2.5256	3.9703
2.0	α (f)	14.4875	14.3241	14.1092	13.8659	13.5662	13.1637	12.6218
	β (f)	0.0571	0.0581	0.0590	0.0600	0.0610	0.0618	0.0620
	ς (f)	1.1850	1.2717	1.4598	1.4316	1.6108	2.0331	0.0217
	ζ (f)	1.2992	1.5111	1.9119	2.1414	2.5027	3.3010	0.4769
2.5	α (f)	12.9451	12.7805	12.5498	12.2784	11.9897	11.5406	11.0608
	β (f)	0.0592	0.0601	0.0611	0.0617	0.0628	0.0631	0.0635
	ς (f)	0.9177	0.9437	0.8172	1.0425	0.9569	0.0155	0
	ζ (f)	0.9668	1.0602	1.2323	1.7869	2.0748	0.4825	0.4726

The fits were performed using the least-square fitting routines available on the Excel solver. The goodness-of-fit between measured data and the values obtained from the Eq. (1) fitted data was assessed using the Kolmogorov-Smirnov (K–S) statistics. The values of K-S relative to the expected values for a 95% confidence level that the two sets of data originate from the same distribution (the null hypothesis) are presented as follow: For 18 MV, the maximum difference between the cumulative distributions, *D*, varied between $0.1500 \leq D \leq 0.2105$ with a corresponding *P-value* of $0.742 \leq P \leq 0.965$. In the other hand for 6 MV, the maximum difference between the cumulative distributions, *D*, is between: $0.0500 \leq D \leq 0.010$ with a corresponding *P-value* =1.00 0 regardless of field sizes and Gamma Putty thickness. In both cases, as P-*value* is greater than 0.05, we accept hypothesis that the two samples come from the same distribution. In other words, the model is statistically consistent with the data.

Table 2. Model parameters α (f), β (f), ς (f), ζ (f) for the 18 MV beam, for all combinations of field size and Gamma Putty thickness. All the parameters were calculated simultaneously by iterative methods.

Thickness (cm)	Parameters	Field sizes(cm^2)						
		10x10	9x9	8x8	7x7	6x6	5x5	4x4
0	α (f)	24.7210	24.7969	24.7969	24.7731	24.6329	24.2070	23.3324
	β (f)	0.0452	0.0461	0.0461	0.0480	0.0489	0.0495	0.0499
	ς (f)	8.14104	8.61756	8.61756	9.52847	9.87521	9.9356	9.5842
	ζ (f)	0.3187	0.3089	0.3089	0.2974	0.2927	0.2930	0.2974
0.3	α (f))	22.7537	22.4730	22.2364	21.9220	21.4907	20.8839	19.8353
	β (f)	0.0460	0.0464	0.0467	0.0471	0.0473	0.0473	0.0466
	ς (f)	0.0872	0	0	0	0	0	0
	ζ (f)	0.0460	0.1954	0.1897	0.1757	0.1811	0.1522	0.1459
0.5	α (f)	21.8694	21.7000	21.4972	21.2068	20.8138	20.2209	19.2573
	β (f)	0.0484	0.0488	0.0494	0.0498	0.0502	0.0503	0.0499
	ς (f)	0	0	0	0	0	0	0
	ζ (f)	0.1161	0.1173	0.1224	0.3187	0.1664	0.1313	0.1130
1.0	α (f)	20.7100	20.5165	20.3010	20.0027	19.5906	19.0024	18.0403
	β (f))	0.0485	0.0491	0.0496	0.0500	0.0503	0.0504	0.0498
	ς (f)	0	0	0	0	0	0	0
	ζ (f)	0.1596	0.1689	0.17375	0.17462	0.16533	0.1633	0.1608
1.5	α (f)	19.5736	19.3963	19.1824	18.8730	18.4472	17.8682	16.8686
	β (f)	0.0501	0.0506	0.0511	0.0515	0.0518	0.0518	0.0508
	ς (f)	0	0	0	0	0	0	0
	ζ (f)	0.17435	0.1809	0.1855	0.2001	0.1833	0.1750	0.1870
2.0	α (f)	17.6898	17.5226	17.3004	16.9889	16.5783	15.9764	15.0592
	β (f)	0.0508	0.0513	0.0518	0.0522	0.0525	0.0523	0.0514
	ς (f)	0	0	0	0	0	0	0
	ζ (f)	0.1899	0.1913	0.1932	0.1940	0.1938	0.1903	0.1830
2.5	α (f)	15.8436	15.6961	15.4650	15.1669	14.7682	14.1924	13.3337
	β (f)	0.0525	0.0531	0.0537	0.0542	0.0545	0.0543	0.0533
	ς (f)	0	0	0	0	0	0	0
	ζ (f)	0.1975	0.1580	0.1622	0.1758	0.1670	0.1635	0.1765

The linear attenuation coefficients μ derived from Eq. (2) for a range of Gamma Putty thicknesses at both beam energies are illustrated using both 3D [Figures 5- 7] and 2D [Figures 8a-n] graphs. At depths below 5cm, the 6 MV beam had the strongest attenuation regardless of Gamma Putty thickness. Smaller field sizes (4×4 and 5×5) also have larger attenuation values at depths greater than 5cm, for both beam energies. For the 6 MV beam especially, we observe a general trend that attenuation factors decrease with increasing field size. This effect might be due to the condition of lateral electronic equilibrium, which is less important for larger field sizes. Note that at or below 10 cm depth, the variation of μ with depth was negligible for both beam energies, and for any

thickness of Gamma Putty. From these plots, we can see that without the Gamma Putty in place, the attenuation factors of the 6 MV beam increase with depth up to 5 cm, then stabilize. For the 18 MV beam, the attenuation factors increase up to 10 cm depth before stabilizing. With a Gamma Putty attenuator, the attenuation factor of the 6 MV beam stabilizes at 1.5cm depth. The total change past this depth is on the order of 0.2%, regardless of field size and attenuator thickness. In contrast, with a Gamma Putty attenuator, the attenuation factor of the 18 MV beam is constant with depth and dependent only on the field size. The attenuation factor tends to decrease gradually for larger field sizes. This is because wider beams generate more in-phantom scattered radiation, which contributes to the dose along the central axis. The lack of lateral electronic equilibrium also decreases the attenuation coefficient observed for small field sizes, since most electrons are scattered away from the central axis. Using the parameterization proposed by Birgani *et al.*[5] in Eq. [2], the coefficient value $\varsigma(f) = 0$ provides the best fit for an 18 MV beam through Gamma Putty, regardless of field size or thickness. The resulting simpler, single-exponential model is also valid for the 18 MV data recorded without any attenuator.

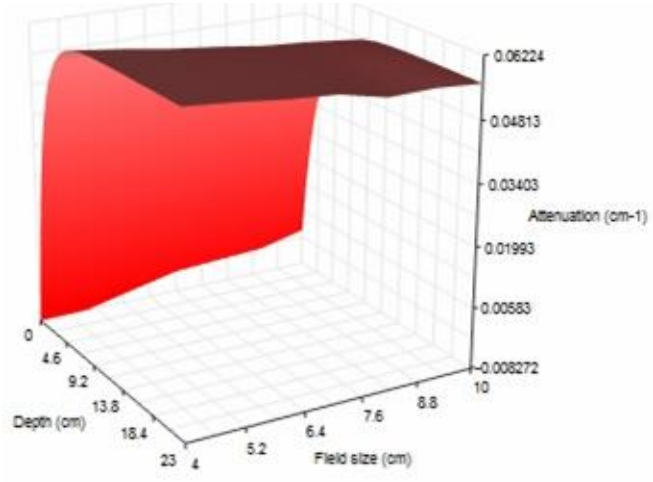

Figure 5a. Variation of the attenuation coefficient with depth and field size for 6 MV photons, without any Gamma Putty.

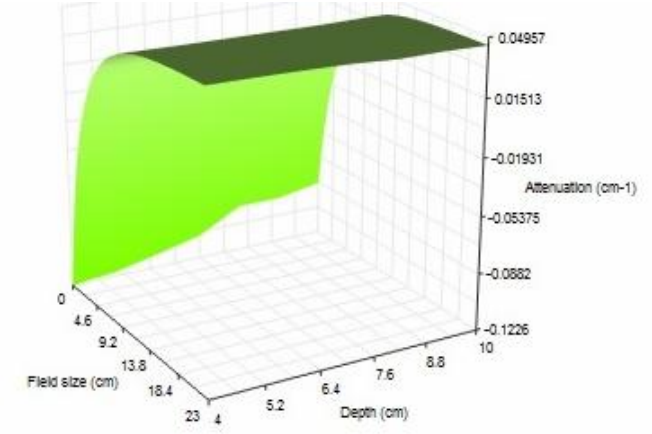

Figure 5b. Variation of the attenuation coefficient with depth and field size for 18 MV photons, without any Gamma Putty.

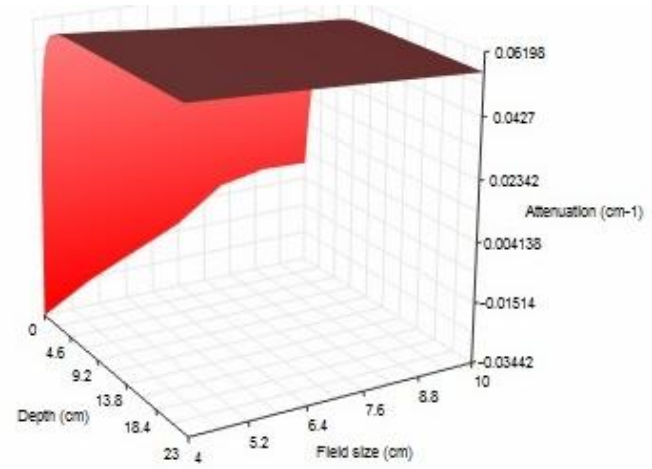

Figure 6a.Variation of the attenuation coefficient with depth and field size for 6 MV photons through 0.5 cm of Gamma Putty.

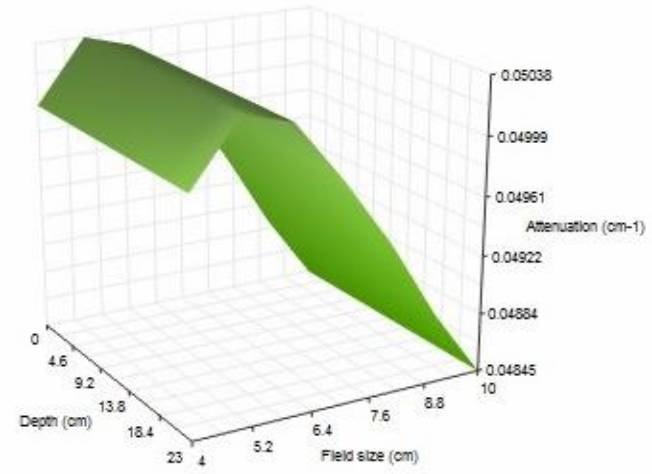

Figure 6b. Variation of the attenuation coefficient with depth and field size for 18 MV photons through 0.5 cm of Gamma Putty

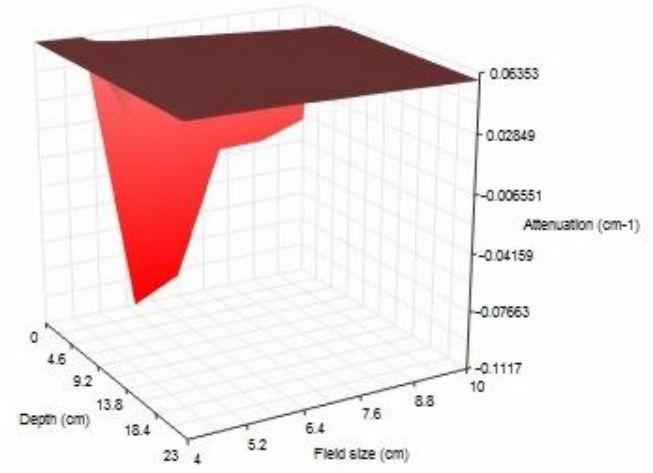

Figure 7a. Variation of the attenuation coefficient with depth and field size for 6 MV photons through 2.5 cm of Gamma Putty.

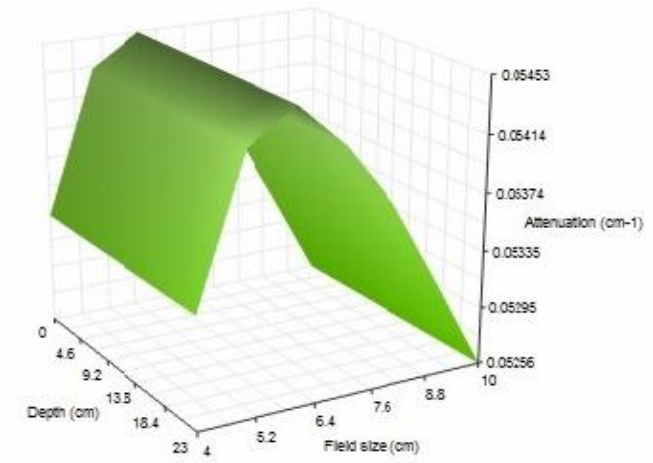

Figure 7 (b). Variation of the attenuation coefficient with depth and field size for 18 MV photons through 2.5 cm of Gamma Putty.

As an alternative to Eq. (2), we modeled the dependence of the attenuation factor on depth and field size for the 18 MV beam using an expression advocated by Weeks *et al* [15]. For a transmission profile of the form exp $(-\mu_{eff}\, t)$, the effective attenuation factor is given by:

$$\mu_{eff} = \mu_0 + \mu_1 f^2 + \mu_2 t A \quad (5)$$

Where f is the equivalent field size and t is the attenuator thickness. The term A is defined as 0 for $f < 10.0$ cm or $(f-10)^{1/3}$ for $f > 10.0$ cm. In our case, since the maximum field size is 10×10 cm^2, the equation becomes

$$\mu_{eff} = \mu_0 + \mu_1 f^2 \quad (6)$$

The best-fit values for μ_0 are given in table 3. The attenuation curves used to fit μ_0 are shown in Fig. 9. This parameterization reproduces the observed attenuation values within 0.05–1% in most cases. A summary of the μ_0 coefficients is shown for several field sizes and Gamma Putty thicknesses in table 3, for the 18 MV beam at 10 cm depth. The parameter μ_1 is a constant, which we evaluate at 0.0001cm^{-1} in all models.

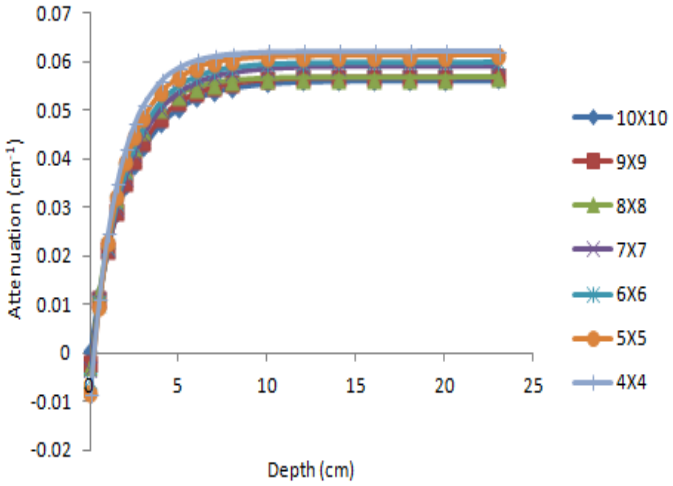

Figure 8a. Attenuation coefficient curves as a function of depth for 6 MV photons without any Gamma Putty, plotted for different field sizes.

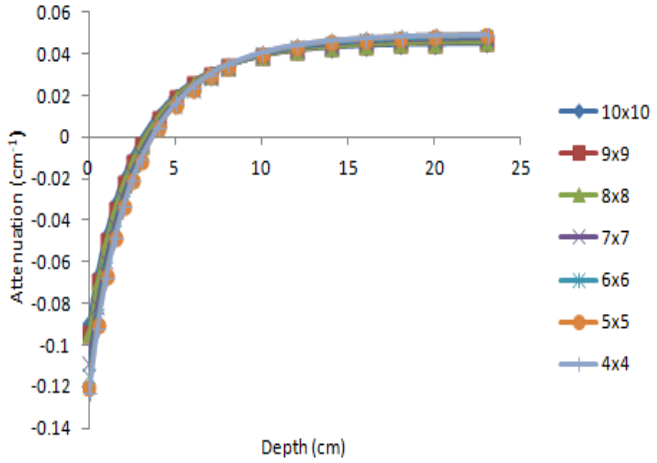

Figure 8b. Attenuation coefficient curves as a function of depth for 18 MV photons without any Gamma Putty, plotted for different field sizes.

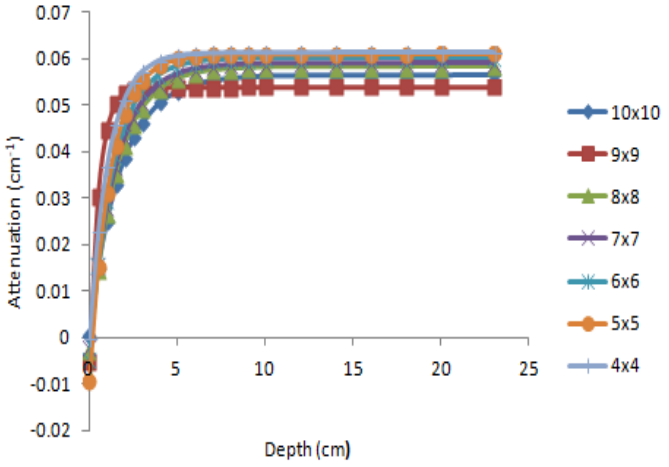

Figure 8c. Attenuation coefficient curves as a function of depth for 6 MV photons through 0.3 cm of Gamma Putty, plotted for different field sizes.

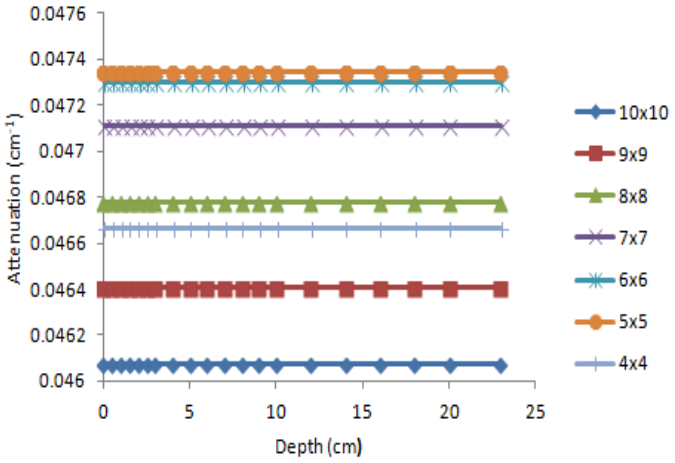

Figure 8d. Attenuation coefficient curves as a function of depth for 18 MV photons through 0.3 cm of Gamma Putty, plotted for different field sizes.

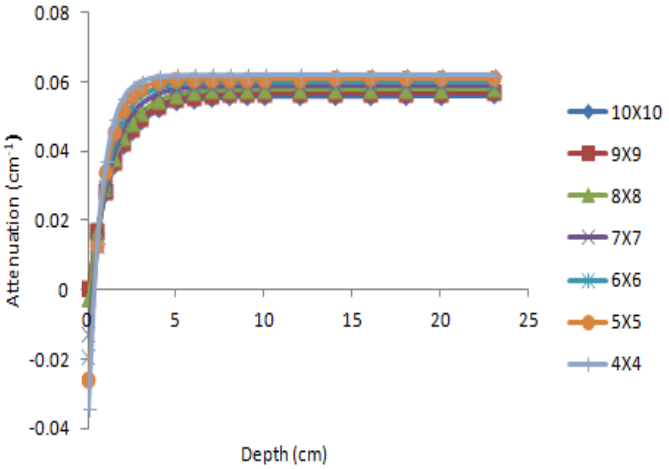

Figure 8e. Attenuation coefficient curves as a function of depth for 6 MV photons through 0.5 cm of Gamma Putty, plotted for different field sizes.

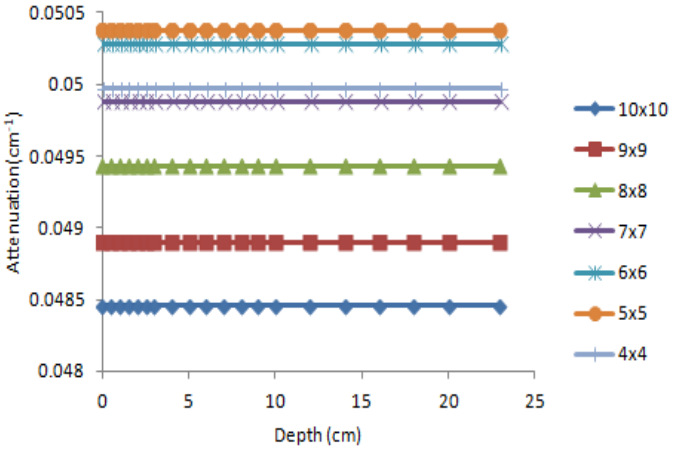

Figure 8f. Attenuation coefficient curves as a function of depth for 18 MV photons through 0.5 cm of Gamma Putty, plotted for different field sizes.

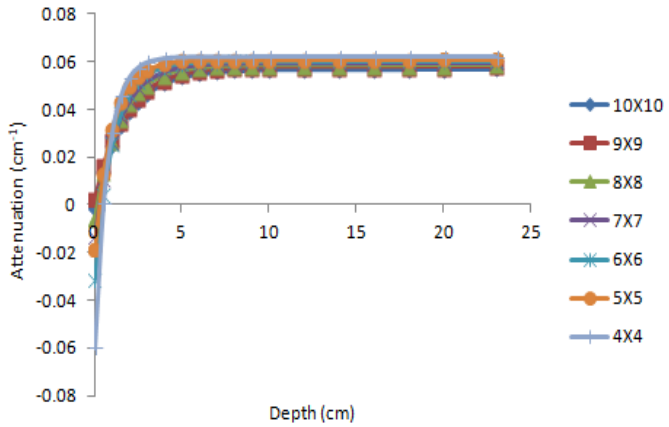

Figure 8g. Attenuation coefficient curves as a function of depth for 6 MV photons through 1.0 cm of Gamma Putty, plotted for different field sizes.

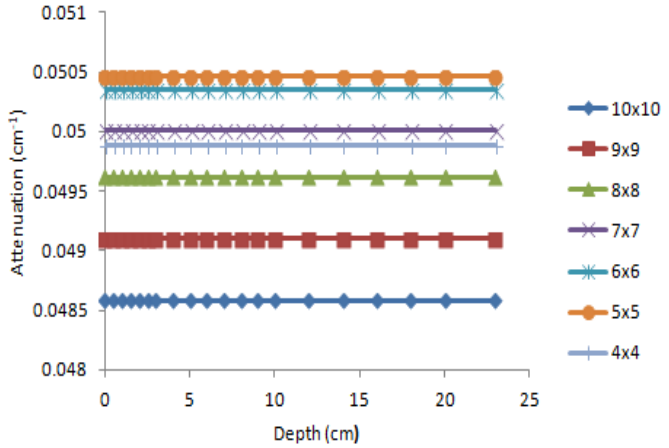

Figure 8h. Attenuation coefficient curves as a function of depth for 18 MV photons through 1.0 cm of Gamma Putty, plotted for different field sizes.

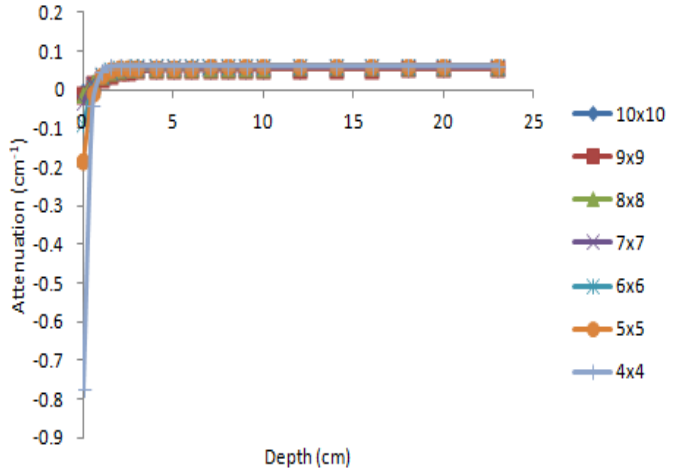

Figure 8i. Attenuation coefficient curves as a function of depth for 6 MV photons through 1.5 cm of Gamma Putty, plotted for different field sizes.

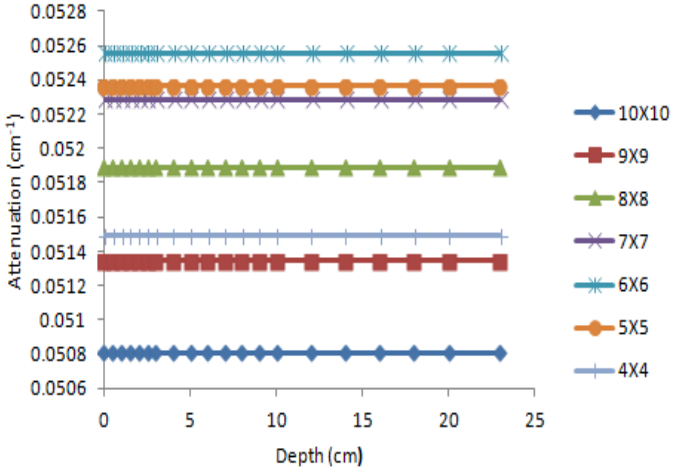

Figure 8l. Attenuation coefficient curves as a function of depth for 18 MV photons through 2.0 cm of Gamma Putty, plotted for different field sizes.

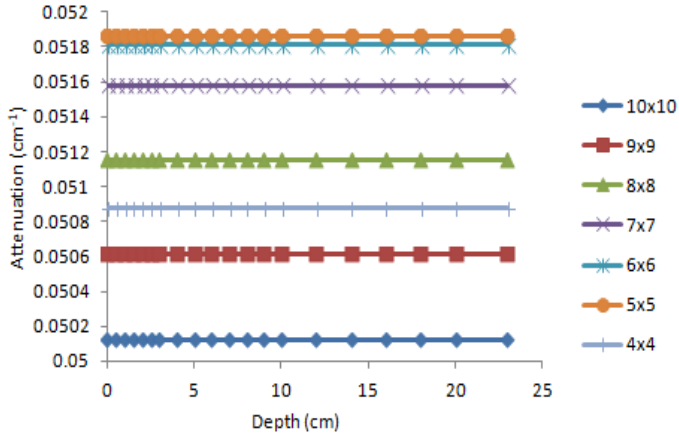

Figure 8j. Attenuation coefficient curves as a function of depth for 18 MV photons through 1.5 cm of Gamma Putty, plotted for different field sizes

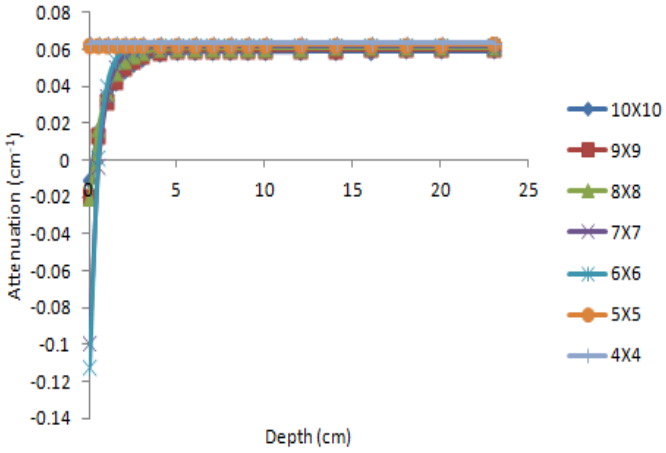

Figure 8m. Attenuation coefficient curves as a function of depth for 6 MV photons through 2.5 cm of Gamma Putty, plotted for different field sizes

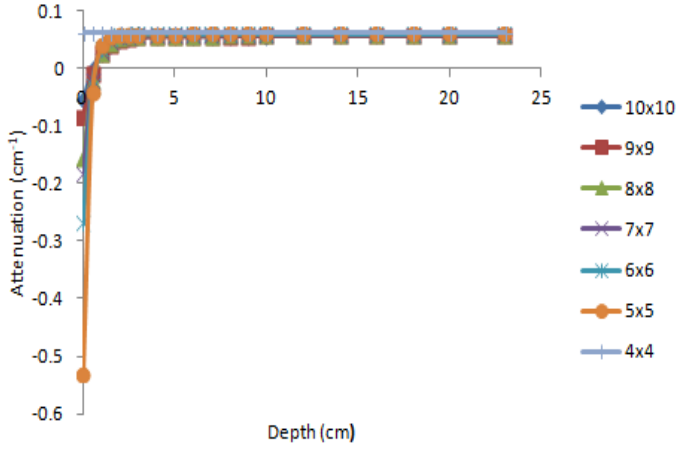

Figure 8k. Attenuation coefficient curves as a function of depth for 6 MV photons through 2.0 cm of Gamma Putty, plotted for different field sizes.

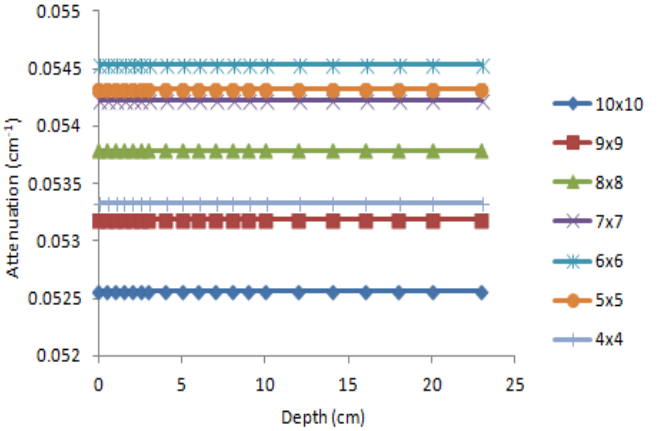

Figure 8n. Attenuation coefficient curves as a function of depth for 18 MV photons through 2.5 cm of Gamma Putty, plotted for different field sizes.

3.2 Beam hardening model

The beam hardening coefficient was determined using equation (3) for each field size and Gamma Putty thickness. Measurements were performed along the central axis at two reference depths: 10 and 20 cm. The second depth is commonly thought to be beyond electron contamination. The model parameters ύ and η were derived by fitting the natural logarithm of the ionization data for these two depths to Eq. (7):

$$\text{Ln (PPD)} = \acute{\upsilon} d\,(1-\eta d) \quad (7)$$

Tables 4 and 5 summarize the results for 6 and 18 MV, respectively.

Table 3. Transmission factors μ_0 of the 18 MV beam at 10 cm depth, for each combination of field size and Gamma Putty thickness. These factors are obtained by fitting the Weeks *et al.* model (6) to the percent ionization dose profiles.

Thickness (cm)	Field sizes (cm^2)						
	10x10	9x9	8x8	7x7	6x6	5x5	4x4
0.3	1.595	1.605	1.612	1.617	1.613	1.612	1.588
0.5	1.038	1.046	1.057	1.048	1.067	1.069	1.051
1.0	0.511	0.516	0.521	0.525	0.528	0.527	0.517
1.5	0.366	0.368	0.372	0.374	0.376	0.374	0.364
2.0	0.272	0.276	0.279	0.282	0.283	0.282	0.275
2.5	0.228	0.231	0.233	0.235	0.237	0.236	0.230

Table 4. Beam hardening (η) and attenuation (ύ) parameters obtained by fitting equation (7) to the log percent depth ionization profiles of the 6 MV photon beam.

Thickness (cm)	Parameters (cm^{-1})	Field sizes (cm)						
		10x10	9x9	8x8	7x7	6x6	5x5	4x4
0.0	ύ	0.4063	0.4042	0.4018	0.3991	0.3956	0.3915	0.3866
	η	0.03794	0.03803	0.03813	0.03827	0.0383	0.03850	0.03866
0.3	ύ	0.3947	0.3919	0.3886	0.3853	0.3822	0.3774	0.3718
	η	0.03814	0.03821	0.03830	0.03841	0.03856	0.03868	0.03881
0.5	ύ	0.3834	0.3812	0.3781	0.3749	0.3704	0.3658	0.3600
	η	0.03825	0.03837	0.03848	0.03858	0.03869	0.03886	0.03900
1.0	ύ	0.3751	0.3728	0.3693	0.3659	0.3610	0.3554	0.34952
	η	0.03852	0.03864	0.03873	0.03888	0.03892	0.03904	0.03917
1.5	ύ	0.3573	0.3544	0.3515	0.3474	0.3433	0.3379	0.3319
	η	0.03838	0.03848	0.03862	0.03871	0.03885	0.03898	0.03913
2.0	ύ	0.3440	0.3409	0.3375	0.3333	0.3281	0.3227	0.3164
	η	0.03888	0.03900	0.03914	0.03923	0.03938	0.03953	0.03970
2.5	ύ	0.3201	0.3164	0.3132	0.3084	0.3032	0.2970	0.3051
	η	0.03907	0.03918	0.03936	0.03946	0.03962	0.03980	0.04047

Table 5. Beam hardening (η) and attenuation (ύ) parameters obtained by fitting equation (7) to the log percent depth ionization profiles of the 18 MV photon beam.

Thickness (cm)	Parameters (cm^{-1})	Field sizes (cm)						
		10x10	9x9	8x8	7x7	6x6	5x5	4x4
0.0	ύ	0.4278	0.4265	0.4248	0.4229	0.4202	0.4165	0.4109
	η	0.03652	0.03656	0.03661	0.03667	0.03673	0.03678	0.03688
0.3	ύ	0.4174	0.4157	0.4139	0.4116	0.4085	0.4047	0.3986
	η	0.03665	0.03670	0.03675	0.03681	0.03687	0.03693	0.0370
0.5	ύ	0.4081	0.4066	0.4044	0.4018	0.3990	0.3947	0.3884
	η	0.03677	0.03682	0.03687	0.03693	0.03701	0.03707	0.03714
1.0	ύ	0.4014	0.3995	0.3973	0.3942	0.3909	0.3863	0.3797
	η	0.03700	0.03704	0.03710	0.03709	0.03717	0.03724	0.03731
1.5	ύ	0.3854	0.3838	0.3813	0.3784	0.3747	0.3698	0.3630
	η	0.03684	0.03692	0.03696	0.03702	0.03707	0.03713	0.03718
2.0	ύ	0.3731	0.3710	0.3685	0.3651	0.3612	0.3562	0.3490
	η	0.03726	0.03732	0.03738	0.03744	0.03750	0.03757	0.03766
2.5	ύ	0.3510	0.3488	0.3457	0.3423	0.3376	0.3321	0.3245
	η	0.03734	0.03742	0.03749	0.03754	0.03761	0.03769	0.03775

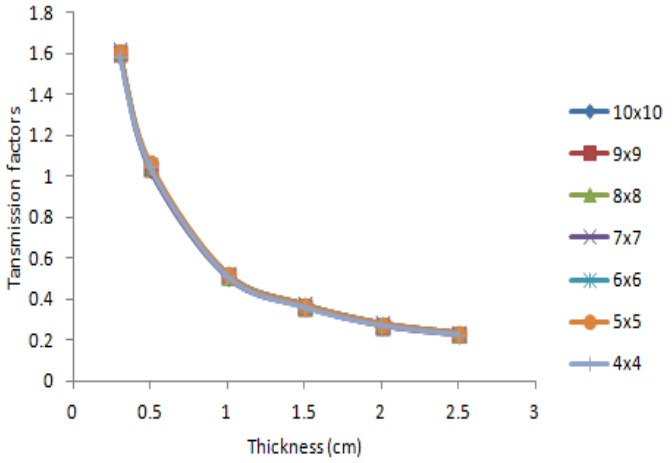

Figure 9. Transmission factors as a function of Gamma Putty thickness, measured at 10 cm depth for 18 MV photons. The transmission factor is nearly independent of field size.

The beam hardening coefficient η increases approximately linearly with decreasing field size [Figures 10a and b]. It also generally increases with the Gamma Putty thickness, although the relationship η (*f*) is more complex [Figures 11a and b]. Also, there is a small difference in the shape of the curves for the smallest low-energy bean ($4\times4cm^2$ at 6 MV), as shown in Figures 10a and b. The best-fit value of η ranges from 0.04047 to 0.03794 cm^{-1} for the 6 MV beam. The total variation at constant beam width ($4\times4cm^2$) is 4.6%, while the total variation at constant Gamma Putty thickness (t = 2.5 cm) is 3.5%. The range of variation is somewhat smaller for the 18 MV beam: 2.3% at a fixed field size of $4\times4cm^2$, and 1.1% at a fixed Gamma Putty thickness (t = 2.5 cm). To aid in determining the beam hardening coefficient for any field size, we report linear regressions for η (*f*) in tables 6 and 7.

Table 6. Linear models of the best-fit η (*f*) parameters in Table 5 for the 6 MV beam

Thickness (cm)	Equation	Error on the slope $x10^{-6}$	R^2
0	-0.0001f+0.0391	8.28	0.9755
0.3	-0.0001f+0.0392	5.46	0.9888
0.5	-0.0001f+0.0395	4.74	0.9926
1.0	-0.0001f+0.0396	4.34	0.9915
1.5	-0.0001f+0.0396	3.44	0.9962
2.0	-0.0001f+0.0402	4.67	0.9940
2.5	-0.0002f+0.041	3.41	0.8767

Table 7. Linear models of the best-fit η (*f*) parameters in Table 5 for the 18 MV beam

Thickness	Equation	Error on the slope x10^{-6}	R^2
0	-5.85E-05f+0.0371	3.190	0.9853
0.3	-5.82E-05f+0.0372	1.420	0.997
0.5	-6.25E-05f+0.0374	2.064	0.9946
1.0	-5E-05f+0.0375	4.907	0.954
1.5	-5.53E-05f+0.0374	1.556	0.9961
2.0	-6.5E-05f+0.0379	2.142	0.9946
2.5	-6.75E-05f+0.038	1.489	0.9976

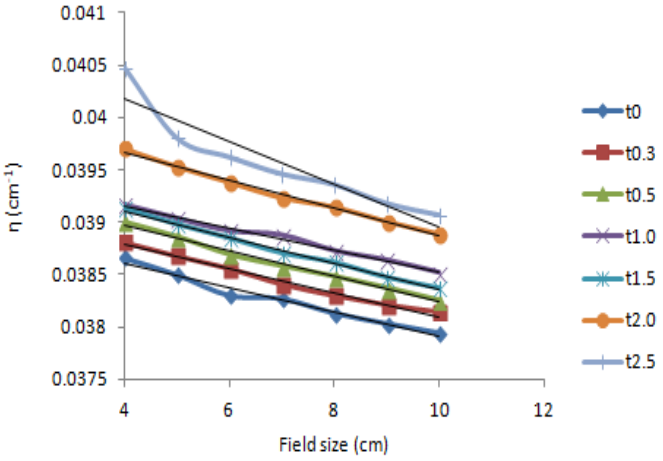

Figure 10a. The beam hardening coefficient η from Eq. (3) as a function of field size, plotted for several Gamma Putty thicknesses (6 MV photons).

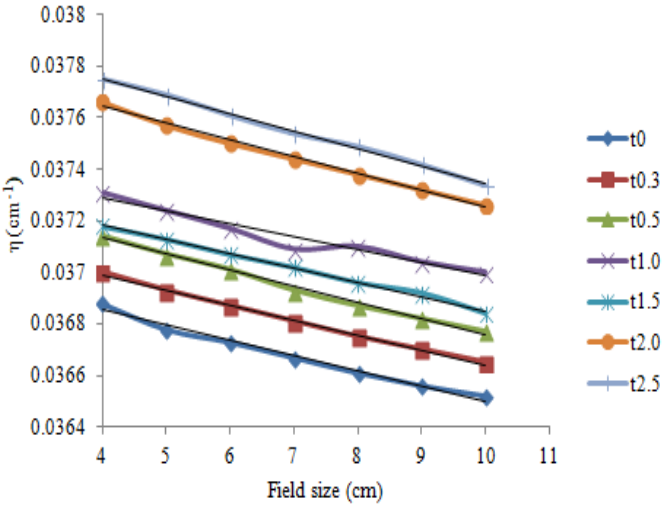

Figure 10b. The beam hardening coefficient η from Eq. (3) as a function of field size, plotted for several Gamma Putty thicknesses (18 MV photons).

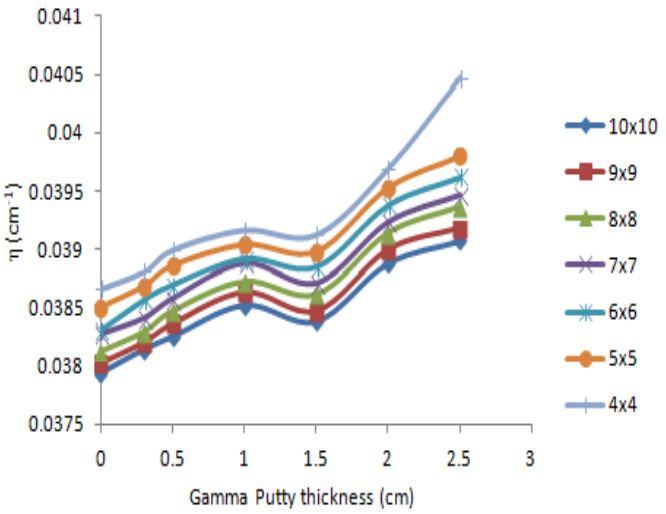

Figure 11a. The beam hardening coefficient η from Eq. (3) as a function of Gamma Putty thickness, plotted for several field sizes (6 MV photons).

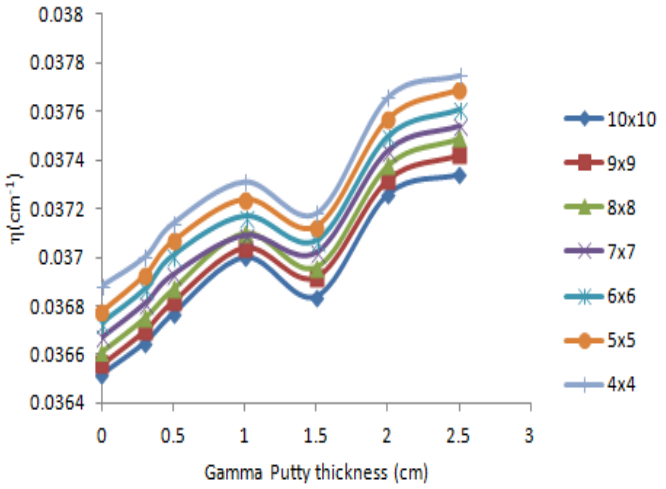

Figure 11b. The beam hardening coefficient η from Eq. (3) as a function of Gamma Putty thickness, plotted for several field sizes (18 MV photons).

Figures 11a and b provide directly measured data showing the beam hardening coefficient η as a function of Gamma Putty thickness. The largest value of η at a given thickness occurs for the 4×4 cm^2 field, regardless of beam energy. The majority of contaminant electrons in this case are produced from the accelerator head, due to the air gap between it and the phantom surface. The discrepancy in η relative to the measurement without any Gamma Putty, as a function of field size, is illustrated in Figs. 12a and b for the 6 MV and 18 MV beams, respectively. The greatest

deviation in η occurs at t = 2.5 cm and the 5×5 cm^2 field size, for both energies.

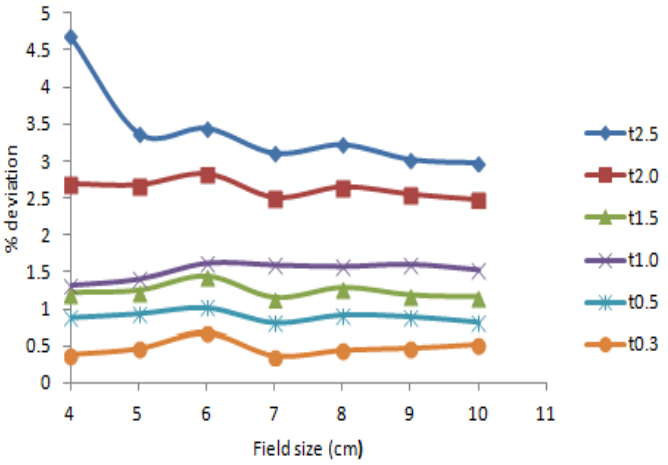

Figure 12a. Differences in corresponding beam hardening coefficients measured with and without Gamma Putty (6 MV photons).

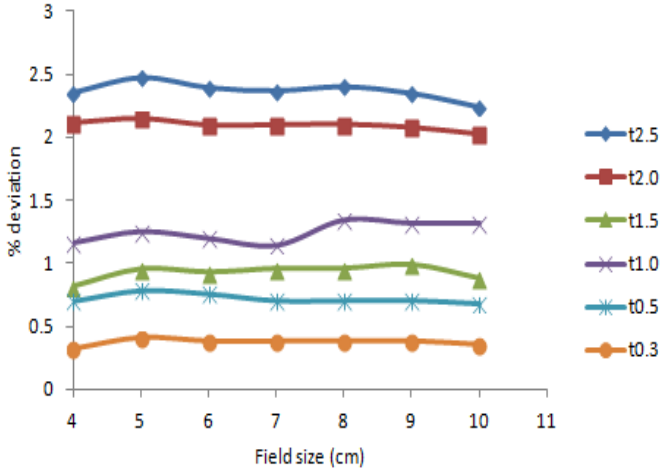

Figure 12b. Differences in corresponding beam hardening coefficients measured with and without Gamma Putty (18 MV photons).

Table 8. Quadratic models of the best-fit ύ (*f*) parameters in Table 3 for the 6 MV beam

Thickness (cm)	R^2	Equation	Abs Sum of Squares x10^{-7}	Sy.x x10^{-3}
0	0.9996	-0.0003f ^{2}+0.0073f +0.3623	1.16	0.1708
0.3	0.9977	-0.0003f ^{2}+0.0072f +0.3472	8.88	0.4712
0.5	0.9997	-0.0003f ^{2}+0.0086f +0.3312	1.10	0.1665
1.0	0.9997	-0.0003f ^{2}+0.0095f +0.3174	1.79	0.2115
1.5	0.9996	-0.0003f ^{2}+0.0089f +0.3019	1.82	0.2135
2.0	0.9999	-0.0003f ^{2}+0.0093f +0.2847	0.62	0.1249
2.5	0.8654	0.0005 f ^{2}-0.0039f +0.3088	523	0.3618

Table 9. Quadratic models of the best-fit ύ (f) parameters in Table 4 for the 18 MV beam.

Thickness (cm)	R^2	Equation	Abs Sum of Squares x10^{-7}	Sy.x x10^{-3}
0	0.9957	-0.0004f ^{2}+0.0082f +0.3848	9.28	0.4817
0.3	0.996	-0.0004f ^{2}+0.0086f +0.3771	10.56	0.4674
0.5	0.996	-0.0004f ^{2}+0.009f +0.3597	11.70	0.5417
1.0	0.9976	-0.0004f^2+0.0095f +0.3491	8.73	0.4674
1.5	0.9984	-0.0005f^2+0.0102f +0.33	6.30	0.3969
2.0	0.9982	-0.0005f ^{2}+0.0104f +0.3152	7.90	0.4441
2.5	0.9989	0.0005f^2-0.0113f +0.2878	5.73	0.3788

It was shown by Kleinschmidt *et al*. [11] that a deviation from linearity in the relation ύ (*f*) implies that the beam spectrum softens as the depth increases and as the attenuation coefficient decreases. The trend lines for ύ (*f*) are shown in Figures 13a and b. A slight curvature, more pronounced for the 18 MV beam, is evident in these figures. However, most of the ύ (*f*) series are well approximated by a second degree order polynomial fitting model. The best-fit parameters of the trend lines are shown in tables 8 and 9, along with the regression coefficient R^2, fitting equations, standard error of the estimate (Sy.x), and absolute sum of squares for 6 and 18 MV, respectively.

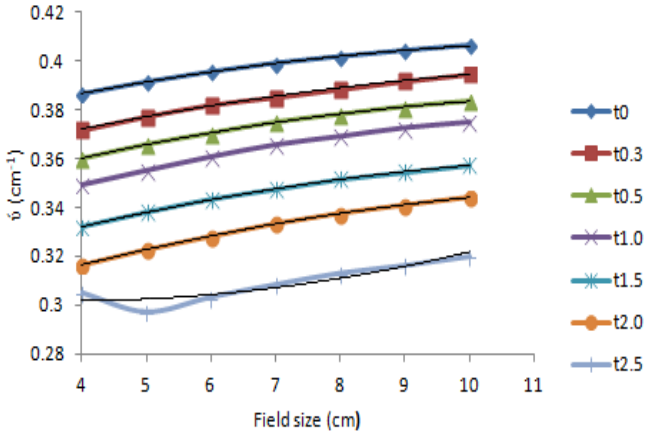

Figure 13a. The attenuation factor coefficient ύ from Eq. (3) as a function of field size (6 MV photons).

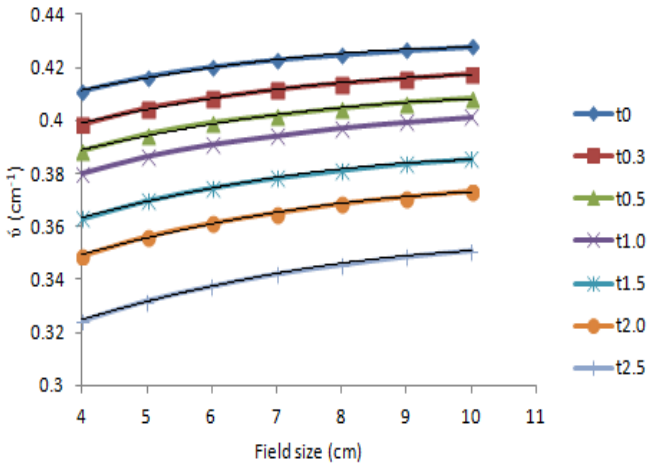

Figure 13b. The attenuation factor coefficient ύ from Eq. (3) as a function of field size (18 MV photons).

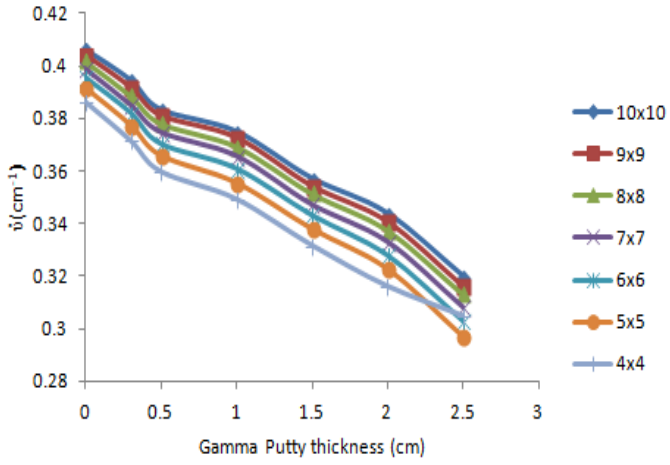

Figure 14a. The attenuation factor coefficient ύ from Eq. (3) as a function of Gamma Putty thickness (6 MV photons).

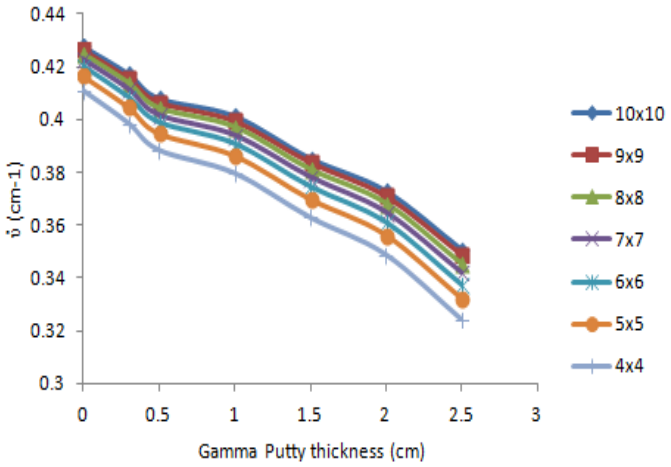

Figure 14b. The attenuation factor coefficient ύ from Eq. (3) as a function of Gamma Putty thickness (18 MV photons).

From theses tables, we can see that $R^2 \geq 0.995$ for all combination of thickness and field size for all energies except for t= 2.5 cm at 6 MV photon beams where $R^2 = 0.8654$. Sy.x which measured the variability of the fitted model is virtually closed to zero suggesting a good fit. Hence, ύ is not constant with respect to field size even though the total variation in this parameter is small. In this study, the attenuation factor ύ ranges from 0.3051 to 0.4063 cm^{-1} for the 6 MV beam and from 0.3245 to 0.4278 cm^{-1} for the 18 MV beam. The observed values of ύ are consistent with those reported by Zhu *et al*. [16] for a 10×10 cm^2 field (ύ = 0.462 cm^{-1}) and by Medina *et al* [17]. Figures 14a and b represent the attenuation coefficient ύ versus Gamma Putty thickness *t* for the 6 MV and 18 MV beams, respectively. As is also evident in Figs. 13 (a) and (b), the attenuation coefficient decreases as the Gamma Putty thickness increases. This trend reveals a gradual hardening of the beam due to more soft photons being absorbed by the Gamma Putty. In addition, these figures show that the linear attenuation coefficient decreases as the field size increases, due to an increase in the scatter component.

Figures 15a and b illustrate the correlation between η and ύ without any Gamma Putty in place for several field sizes. Despite the large deviations from the fitting curve observed in ύ and η for some field sizes, the two parameters are clearly strongly correlated. In this model, a large value of ύ is

always compensated by a large value of η and vice versa, as argued by Sauer *et al* [18].

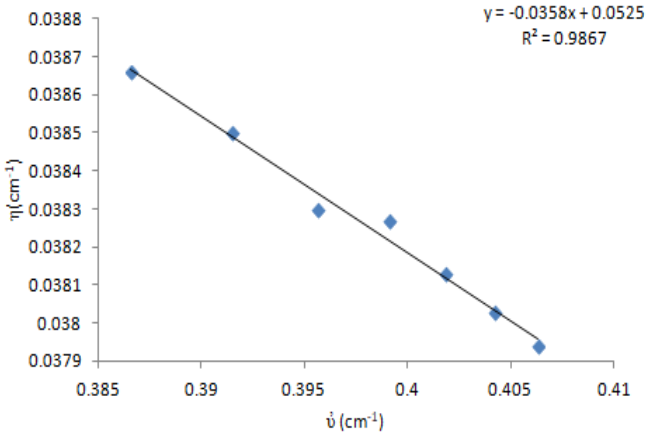

Figure 15a. Correlation between the attenuation coefficient ύ and the beam hardening coefficient η derived from Eq. (7), for 6 MV photons. The different points correspond to different field sizes, without using any Gamma Putty

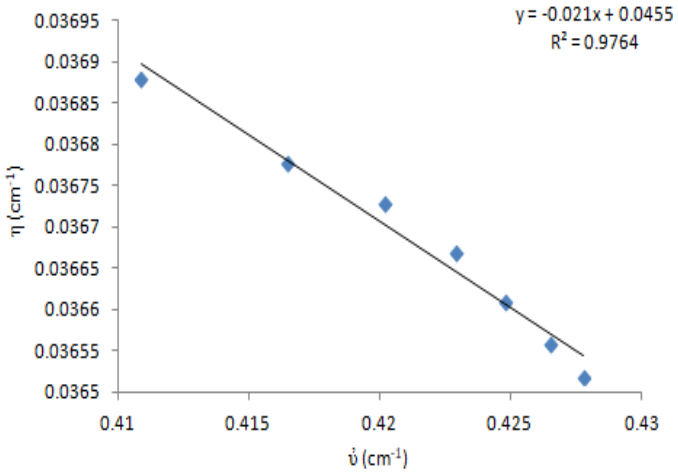

Figure 15b. Correlation between the attenuation coefficient ύ and the beam hardening coefficient η derived from Eq. (7), for 18 MV photons. The different points correspond to different field sizes, without using any Gamma Putty

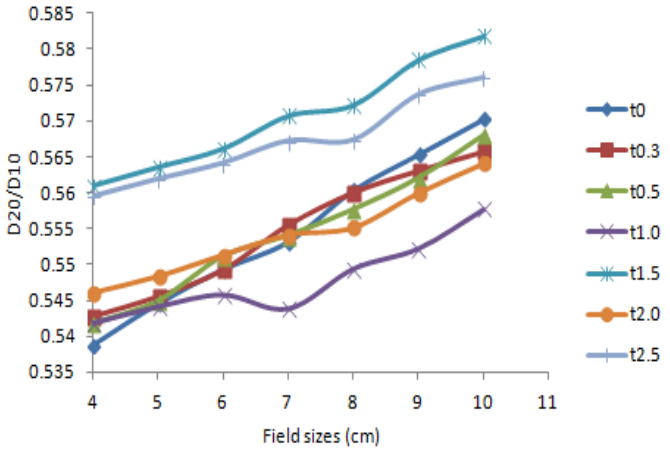

Figure 16a. D_{20}/D_{10} as a function of field size and Gamma Putty thickness, for 6 MV photons

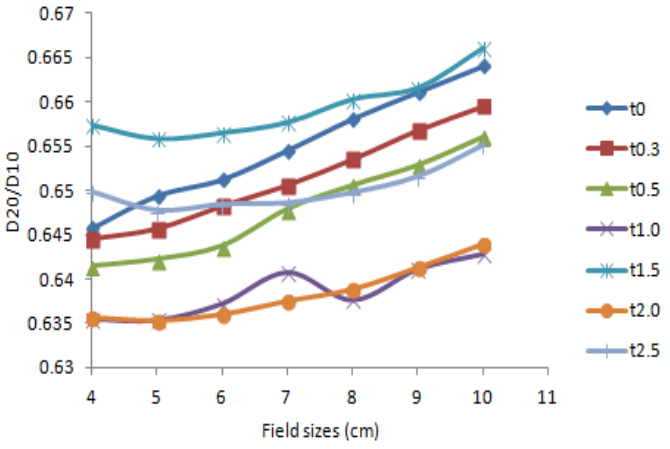

Figure 16b. D_{20}/D_{10} as a function of field size and Gamma Putty thickness, for 18 MV photons

Table 10. D_{20}/D_{10} values for different field sizes and thicknesses of Gamma Putty, for the 6 MV photon beam.

Field size (cm^2)	Thickness (cm)							% error
	t0	t0.3	t0.5	t1.0	t1.5	t2.0	t2.5	
10x10	0.57028	0.56571	0.56795	0.55777	0.58186	0.5641	0.5761	1.022825
9x9	0.56536	0.56306	0.56202	0.55228	0.57853	0.56	0.57372	1.480363
8x8	0.56037	0.56	0.55762	0.54943	0.57225	0.55513	0.56737	1.249134
7x7	0.55319	0.55545	0.554	0.5438	0.57075	0.55409	0.56723	2.521317
6x6	0.54935	0.54919	0.55108	0.54576	0.56618	0.5513	0.5641	2.66462
5x5	0.54455	0.54546	0.54487	0.5441	0.56361	0.5483	0.56187	3.146651
4x4	0.53875	0.54265	0.54171	0.54177	0.56101	0.54599	0.55944	3.780522
% error	5.686059	4.158149	4.734025	2.921089	3.654058	3.268006	2.937826	

Table 11. D_{20}/D_{10} values for different field sizes and thicknesses of Gamma Putty, for the 18 MV photon beam.

Field size (cm^2)	Thickness (cm)							% error
	t0	t0.3	t0.5	t1.0	t1.5	t2.0	t2.5	
10x10	0.66402	0.65956	0.65606	0.64274	0.66608	0.64389	0.65521	1.344286
9x9	0.6611	0.65684	0.65287	0.64107	0.66163	0.64125	0.65164	1.450313
8x8	0.65809	0.65354	0.65058	0.63763	0.66034	0.63881	0.64977	1.280501
7x7	0.65453	0.65059	0.6479	0.6407	0.65775	0.63747	0.64859	0.91759
6x6	0.65126	0.64822	0.64373	0.63722	0.65658	0.63598	0.64842	0.440151
5x5	0.64943	0.64564	0.6422	0.6354	0.65591	0.63528	0.64773	0.263455
4x4	0.64574	0.64448	0.64143	0.63552	0.65746	0.63564	0.64987	-0.64053
% error	2.7915	2.315183	2.258945	1.130575	1.306957	1.291965	0.821935	

3.3 Beam quality analysis

In this study, D_{20}/D_{10} (beam quality) values were measured along the CAX. The effects of attenuator thickness and field size on D_{20}/D_{10} are illustrated in Figures 16a and b, for the 6 MV and 18 MV beams respectively. D_{20}/D_{10} increases with field size regardless of attenuator thickness, and is energy-dependent. Figures 17a and b show the deviations between D_{20}/D_{10} measured with and without Gamma Putty for the 6 and 18 MV beams, respectively. These plots clearly show that the largest positive difference always occurs for the smallest field size (4×4 cm^2) for both energies. This behavior is due to electron contamination. In contrast, the deviations for wide fields are low or negative. The deviation gradually decreases with increasing field size for all thicknesses of Gamma Putty and both beam energies. For larger fields this hardening is less noticeable, due to the greater contribution from low-energy scatter generated in the Gamma Putty. The D_{20}/D_{10} values obtained for each combination of Gamma Putty thickness and field size are given in tables 10 and 11, for the 6 MV and 18 MV beams respectively.

The ratio D_{20}/D_{10} has the advantage of being directly related to the linear attenuation coefficient μ (z, f), of the photon beam. Plotting the attenuation coefficient μ against D_{10}/D_{20} results in a linear fit, similar to that provided by Brahme *et al*. [19]:

$$\mu_d = d^* \ln (D_{10}/D_{20}) \quad (8)$$

where d =0.1cm^{-1} for a beam energy below 40 MV. In our case, when we plot μ against D_{10}/D_{20} for different combinations of Gamma Putty thickness and field size, we find that the relationship is linear and that its slope is consistent with the result of Brahme *et al* [19].

μ_d = (0.137967± 0.032364) ×ln (D_{10}/D_{20}) − (0.01509±0.018379) for 6 MV (all field sizes)

μ_d = (0.11928± 0.031587) ×ln (D_{10}/D_{20}) − (0.00088 ± 0.011898) for 18 MV (field sizes greater than 5×5 cm^2).

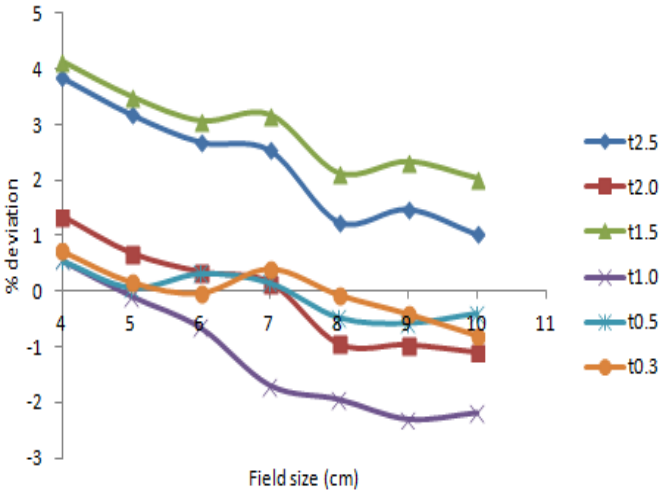

Figure 17a. Differences in corresponding beam qualities D_{20}/D_{10} measured with and without Gamma Putty (6 MV photons).

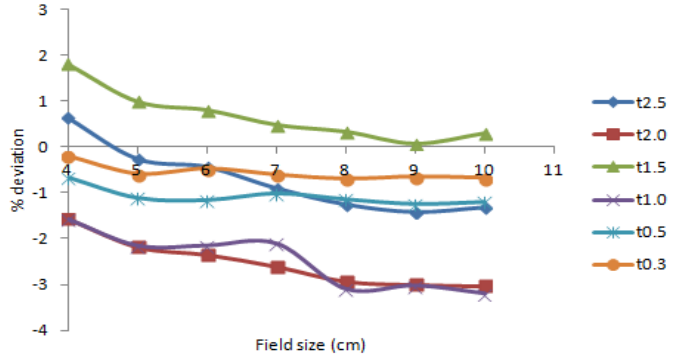

Figure 17b. Differences in corresponding beam qualities D_{20}/D_{10} measured with and without Gamma Putty (18 MV photons).

3.4 Electron contamination model

The effect of electron contamination was evaluated by fitting all of the percent depth ionization data to the bi-exponential expression provided by Brahme *et al*. [19] in Eq. (4). Tables 12 and 13 list the best-fit parameters.

Table 12. Fitted parameters of equation (4) for 6 MV photon beams. The factors v and K together describe the value of the bremsstrahlung surface dose $K(1.0-v)$, where K is constant for a given field size and attenuator thickness.

Thickness (cm)	Fitted Parameters	10x10	9x9	8x8	7x7	6x6	5x5	4x4
0	K	21.87772	21.66409	21.08901	21.28797	20.92099	20.53544	19.98598
	A	0.056145	0.056969	0.056809	0.059217	0.060019	0.061284	0.062234
	B	0.493721	0.517943	0.604005	0.522729	0.559051	0.599272	0.648946
	v	0.113055	0.113613	0.098056	0.118893	0.116373	0.114323	0.107306
0.3	K	20.18067	19.07554	19.7142	19.4268	19.08361	18.66632	18.00713
	A	0.05662	0.053879	0.058295	0.059182	0.060104	0.061056	0.061412
	B	0.593194	0.593194	0.675233	0.699577	0.768451	0.873324	0.941082
	v	0.094467	0.094467	0.090203	0.087199	0.083815	0.080018	0.065403
0.5	K	18.62052	18.4718	18.26015	17.98474	17.65227	17.24982	16.7518
	A	0.056051	0.057104	0.05814	0.059133	0.060094	0.061094	0.061979
	B	0.675552	0.675096	0.765815	0.90366	1.028296	1.176536	1.368423
	v	0.081777	0.08248	0.078776	0.078307	0.07571	0.072259	0.068724
1.0	K	17.64081	17.46082	17.17672	16.90415	16.54668	16.07238	15.57884
	A	0.056957	0.057877	0.058671	0.059622	0.060412	0.061092	0.061948
	B	0.584016	0.597803	0.6991	0.754952	0.827726	0.951989	1.137125
	v	0.093331	0.089995	0.086578	0.087953	0.080247	0.073657	0.072263
1.5	K	16.26222	16.11022	15.88208	15.61257	15.28191	14.89423	14.38337
	A	0.057007	0.058015	0.058877	0.059744	0.060653	0.061558	0.062195
	B	0.96216	1.021091	1.125578	1.301114	1.55671	1.729819	1.909042
	v	0.061074	0.062927	0.060658	0.058837	0.05773	0.054806	0.054055
2.0	K	14.55894	14.32213	14.18364	13.93671	13.56102	13.22835	12.66158
	A	0.057565	0.058104	0.059535	0.060471	0.061045	0.062345	0.06191
	B	0.931657	1.532855	1.153093	1.242	2.531725	1.586059	1.505766
	v	0.073904	0.090395	0.074095	0.069725	0.117175	0.051503	0.046912
2.5	K	12.89841	12.73265	12.58046	12.30105	12.02733	11.59303	11.0597
	A	0.058978	0.05999	0.061244	0.06223	0.063237	0.06324	0.063524
	B	0.997841	1.033778	1.14725	1.481727	1.622115	1.236874	0.570027
	v	0.067474	0.063474	0.066973	0.056234	0.063359	0.023304	8.29E-05

Table 13. Fitted parameters of equation (4) for 18 MV photon beams. The factors *K* and *v* together describe the value of the bremsstrahlung surface dose *K* (1.0−*v*), where *K* is constant for a given field size and attenuator thickness.

Thickness (cm)	Fitted Parameters	10x10	9x9	8x8	7x7	6x6	5x5	4x4
0	K	24.72169	24.79765	24.78656	24.77456	24.63145	24.20885	23.33099
	A	0.045255	0.046144	0.046975	0.047986	0.048918	0.049566	0.049913
	B	0.318686	0.308967	0.303185	0.297432	0.292795	0.292965	0.297492
	v	0.329339	0.347558	0.3655	0.384663	0.400864	0.410498	0.410747
0.3	K	24.29825	24.10831	23.94529	23.62855	23.21535	26.53099	25.83611
	A	0.046071	0.046404	0.046773	0.047109	0.047299	0.047336	0.046666
	B	0.046069	0.0464	0.046769	0.047105	0.047294	0.047311	0.046671
	v	0.06716	0.067832	0.071368	0.072228	0.074295	0.212846	0.232261
0.5	K	23.89424	23.23229	23.53838	22.52136	22.97806	21.59655	19.4083
	A	0.048454	0.048898	0.049427	0.04988	0.050282	0.050376	0.049972
	B	0.048447	0.048891	0.049416	0.049876	0.050282	0.050366	0.049975
	v	0.084744	0.065952	0.086711	0.058366	0.094186	0.063691	0.007776
1.0	K	20.71001	20.55032	20.33123	20.03273	19.6194	19.02495	18.05548
	A	0.048583	0.049244	0.049746	0.050139	0.050475	0.050566	0.049953
	B	0.199702	0.18873	0.189598	0.207291	0.207845	0.206801	0.197945
	v	0	0	0	0	0	0	0
1.5	K	19.6189	19.43961	19.22642	18.91239	18.48456	17.89623	16.88875
	A	0.050326	0.050811	0.051358	0.051763	0.051994	0.052002	0.050985
	B	0.454513	0.209504	0.211881	0.212065	0.210336	0.212409	0.195785
	v	0	0	0	0	0	0	0
2.0	K	17.68982	17.52265	17.30046	16.989	16.57842	15.97649	15.05934
	A	0.050811	0.051346	0.051891	0.052287	0.052557	0.052364	0.05149
	B	0.228143	0.228821	0.229567	0.229089	0.227309	0.222635	0.209736
	v	0	0	0	0	0	0	0
2.5	K	15.8436	15.67365	15.44579	15.14431	14.74585	14.17082	13.31799
	A	0.05256	0.053059	0.05368	0.054092	0.054397	0.054184	0.053224
	B	0.228039	0.227702	0.226415	0.222587	0.213816	0.210706	0.210708
	v	0	0	0	0	0	0	0

Figures 18a and b show the bremsstrahlung electron contamination measured at the surface, *K* (1.0−*v*), as a function of field size and Gamma Putty thickness. *K* (1.0−*v*) increases steadily with field size. For small field sizes, air is the main source of contaminating electrons. Zhu *et al*. [20] suggested that 70–80% of bremsstrahlung originates from accelerator head accessories such as jaws, scattering foils, and the transmission ion chamber. The remaining percentage comes from beam modifiers such as the Gamma Putty. The largest values of *v* are 0.11 and 0.41, for the 6 MV and 18 MV beams, respectively. Both of these values were observed without any attenuator. As the Gamma Putty thickness increases, *v* and *K* (1.0−*v*) both decrease. The observed trends in *K* (1.0−*v*) are approximately linear, decreasing with Gamma Putty thickness and increasing with field size. The parameter *v* is dependent on field size for the 6 MV beam. However, for the 18 MV beam, *v* takes the value 0 for all Gamma Putty thicknesses greater than 0.5 cm. Medina *et al*. [17] stipulated that electrons scattered from the linac treatment head are more energetic than those scattering in air, due to the higher atomic number of the scattering nuclei. The contamination by electrons generated from the air by the 18 MV beam decreases rapidly with depth, resulting in lower values of *v*.

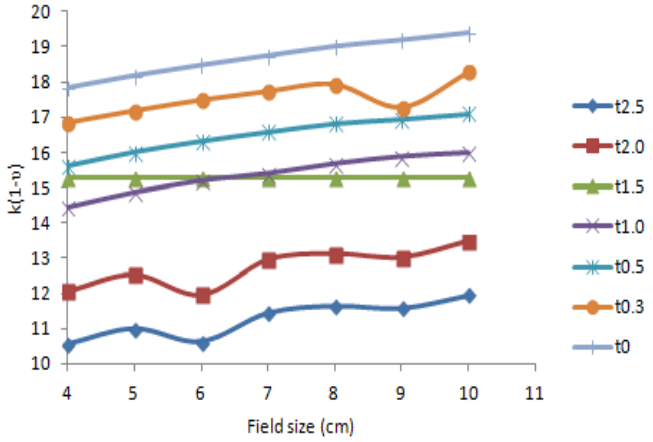

Figure 18a. Relative bremsstrahlung surface doses for 6 MV photons.

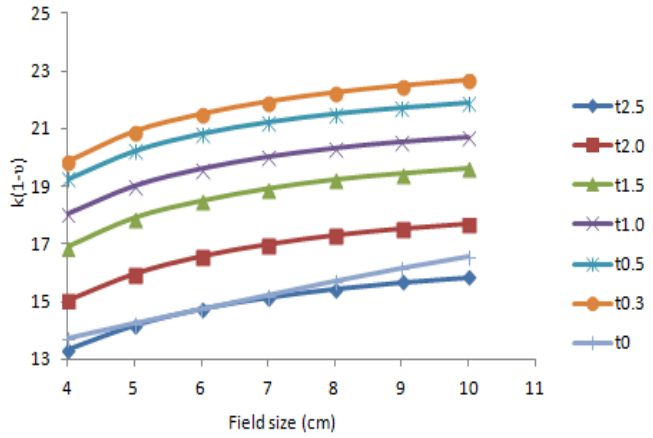

Figure 18b. Relative bremsstrahlung surface doses for 18 MV photons

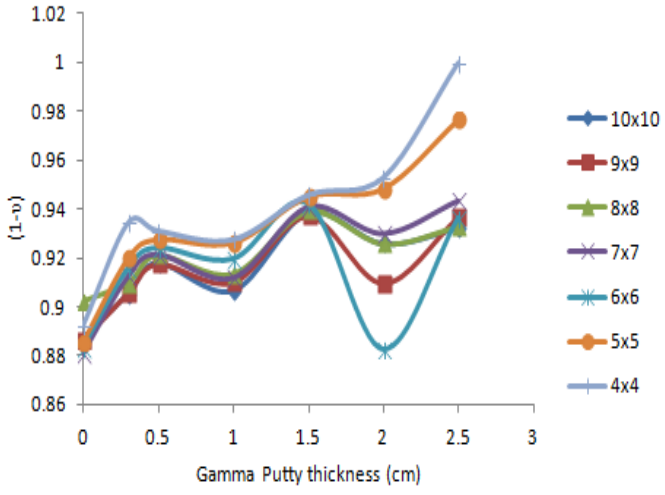

Figure 19a. Electron contamination factors (1−*v*) as a function of Gamma Putty thickness for 6 MV photons.

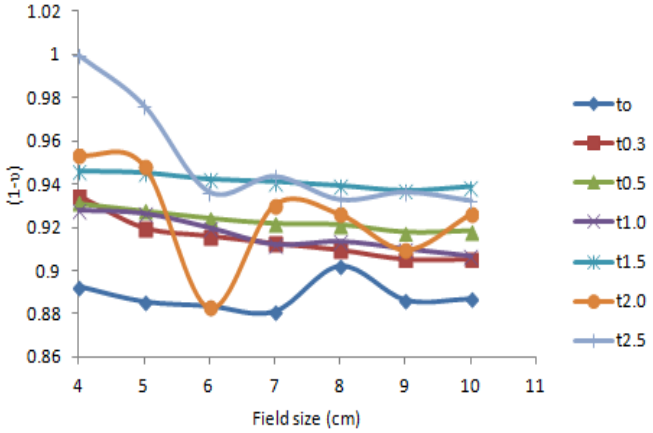

Figure 19b. Electron contamination factors (1−*v*) as a function of field size for 6 MV photons.

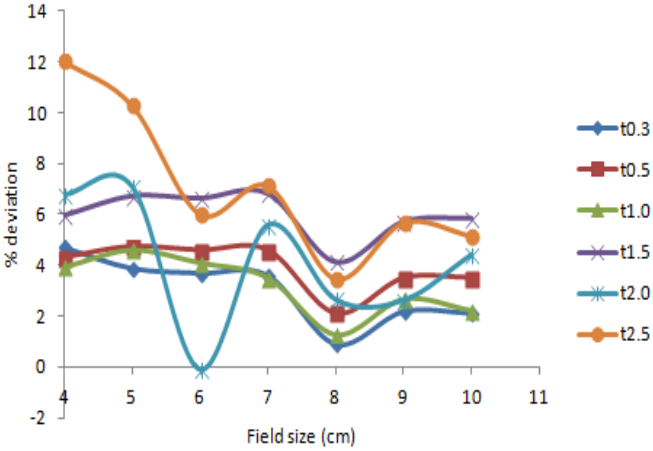

Figure 19c. Differences in electron contamination factors (1−*v*) measured with and without Gamma Putty (6 MV photons).

The source of electron contamination for the system can be characterized by (1−*v*). The values of (1−*v*) obtained for a 10×10 cm^2 field are 0.886 and 0.6706 for the 6 MV and 18 MV beams respectively, without any attenuator. These values are comparable to those defined by Medina *et* al. [17] who reported a range of 0.7 to 2.8 cm^{-1} for 6 MV and 0.7 to 1.2 cm^{-1} for 18 MV. For a Gamma Putty thickness greater than 0.5 cm, however, we obtain v = 0. This suggests that electrons generated in the air are less important than those produced by the linac treatment head. Electrons generated in the air are much more important for the 6 MV beam than for the 18 MV beam. For both energies, electrons generated in the air are less energetic than those produced in the linac treatment head. Especially for 18 MV, treatment head electrons are

more pronounced due to pair production. For larger field sizes and higher energies, the surface dose is abundant compared to electrons generated in the air.

It seems that, for a small field size, the air column between the treatment head where the source is located and the phantom-attenuator complex supplied an increasing portion of contaminating electrons. This result is on full display with the 6 MV beam [Figure 19b], where the 4x4 cm^2 field has the highest $(1-v)$ for all Gamma Putty thicknesses. For larger field sizes, the treatment head (consisting of target, collimator jaws, flattening filters, and monitor chambers) decreases the amount of electron contamination. The proportion $(1-v)$ also decreases as the Gamma Putty thicknesses increases [Fig. 19 (a)]. For field sizes between 7 and 10 cm, there is an opposing process between the two events rendering $(1-v)$ fairly constant.

Table 14. 6MV Electron contamination change with variable Gamma Putty thickness for field sizes 4-10.

Thickness (cm)	Field size (cm)							% error
	10x10	9x9	8x8	7x7	6x6	5x5	4x4	
0	0.8869	0.8864	0.9019	0.8811	0.8836	0.8856	0.8927	0.6472
0.3	0.9055	0.9055	0.9098	0.9128	0.9162	0.9199	0.9346	3.1767
0.5	0.9182	0.9175	0.9212	0.9216	0.9243	0.9278	0.9313	1.4140
1.0	0.9067	0.9100	0.9134	0.9120	0.9197	0.9263	0.9278	2.2986
1.5	0.9389	0.9371	0.9393	0.9412	0.9423	0.9452	0.9460	0.7456
2.0	0.9261	0.9096	0.9259	0.9303	0.8830	0.9485	0.9531	2.9175
2.5	0.9325	0.9365	0.9333	0.9438	0.9366	0.9767	0.9999	7.0842
% error	3.2159	3.0915	2.0335	4.2699	3.4376	5.0595	5.1083	

Table 15. 18MV Electron contamination change with variable Gamma Putty thickness for field sizes 4-10.

Thickness (cm)	Field size (cm)							% error
	10x10	9x9	8x8	7x7	6x6	5x5	4x4	
0	0.6707	0.6524	0.6345	0.615337	0.5991	0.5895	0.5892	13.0977
0.3	0.9328	0.9322	0.9286	0.9278	0.9257	0.787154	0.767739	18.6344
0.5	0.9153	0.9340	0.9133	0.9416	0.9058	0.9364	0.9922	-8.2399
1.0	1	1	1	1	1	1	1	0
1.5	1	1	1	1	1	1	1	0
2.0	1	1	1	1	1	1	1	0
2.5	1	1	1	1	1	1	1	0
% error	35.3652	37.3222	39.5050	41.5227	43.6355	45.5172	45.28479	

For 18 MV, the scenario seems different. As the field size increases, $(1-v)$ remains almost constant after 6×6 cm^2 [Figure 20b], and fairly constant for Gamma Putty thickness $t \geq 1.0$ cm. This suggests that the effect of field size is not noticeable. However, as the Gamma Putty thickness increases [Fig. 20 (a)], we see that $(1-v)$ is still larger than the case without any Gamma Putty (t=0), and that this effect is significant for t>1.0 cm. Furthermore, the change in electron contamination for the 6 MV beam compared to the case of no Gamma Putty attenuator is highest for 4×4 cm^2 fields, and also highest for the greatest thickness of Gamma Putty [Figure 19c and table 14]. In contrast, for the 18 MV beam, no trend is apparent [Figure 20c and table 15]. However, for t >0.5 cm a relatively large difference was achieved at 4×4 cm^2, which decreased as the field size increased, broadly confirming our previous assertion that other components of the linac are mainly responsible for electron contamination in spite of attenuator presence. This may be attributed to radiation

emission via the small angle and small scattering power associated with higher energy beams.

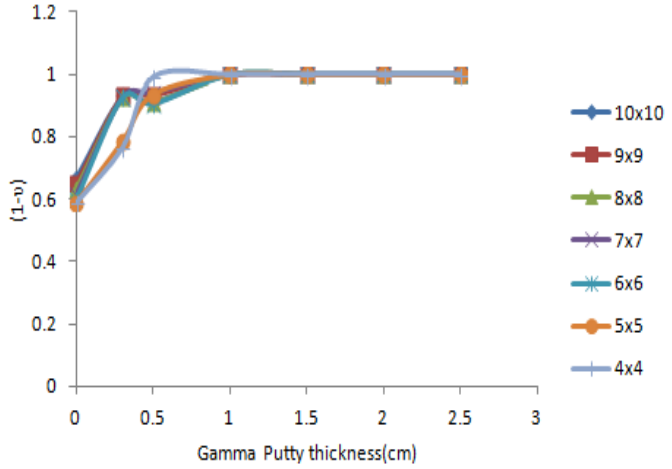

Figure 20a. Electron contamination factors (1−*v*) as a function of Gamma Putty thickness for 18 MV photons.

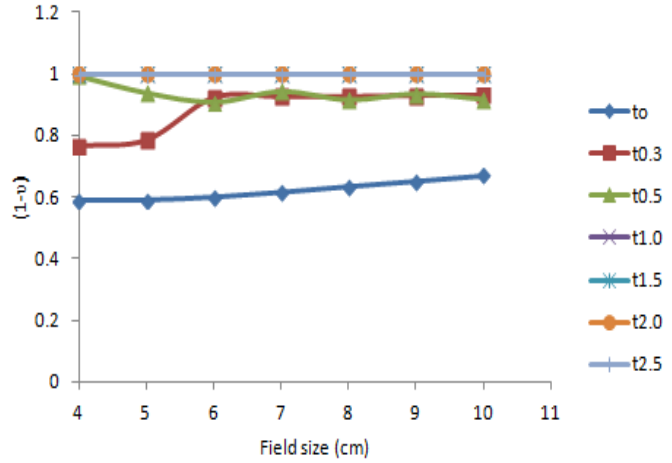

Figure 20b. Electron contamination factors (1−*v*) as a function of field size for 18 MV photons.

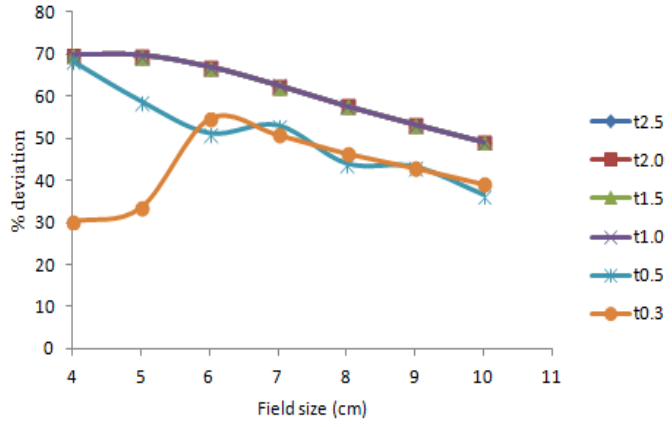

Figure 20c. Differences in electron contamination factors (1−*v*) measured with and without Gamma Putty (18 MV photons).

4. Discussion

Radiotherapy is often conducted using broad-beam geometry. All experiments and calculations in this study were performed under this condition. The attenuation coefficients were derived from percent ionization depth dose values using an analytical expression that describes the variation of dose with depth in a homogeneous medium. We measured attenuation coefficients μ for a range of field sizes and Gamma Putty thicknesses. The values of μ observed at the surface (0 cm depth) for a 10×10 cm^2 field are in the same range as those reported by Xiao *et al.*[21] evaluated at 0.0467cm^{-1} and 0.0321cm^{-1} for 6 and 18 MV, respectively. In this study, for the 6 MV beam without any Gamma Putty, we found μ = 0.04365±0.016838 cm^{-1}. For the 18 MV beam under the same conditions, we found μ = 0.00876 ± 0.041379 cm^{-1}.

The beam hardening coefficient η was found to be small for both beam energies and all field sizes considered in this study. However, this parameter has a large error range because it is determined using only two fixed depths. Even so, the range of variation in our measured values of η is very small: for the 6 MV beam, the coefficient of variation among fitted values for the different field sizes is on the order of 0.6% for all Gamma Putty thicknesses, except for the 2.5 cm Gamma Putty attenuator where the coefficient of variation was closer to 1.0%. In contrast, for 18 MV there is even more consistency with the coefficient of variation of η evaluated at 0.3%. For any given field size, energy and thickness, there is an independent linear relationship between η and ύ, whose parameters are reported in tables 3 and 4.

Brahm and Andreo [14] stated that all photon beams used in radiotherapy are to some extent contaminated by a combination of electrons and positrons generated through the photoelectric effect, Compton scattering, and pair production processes. These interactions change the shape of the buildup region, thus impacting the photon depth dose curve. For the 6 MV beam, air between the linac source and the patient is the main source of secondary electrons. For the 18 MV beam, the flattening filter is the main source of secondary electrons. These scattering events are exacerbated by the nature of the attenuator. Gamma Putty contains 8.94%

hydrogen by weight, which contributes to its relatively low electron density (Z/A). However, the atomic number of Gamma Putty is high (90% bismuth, Z=83), which enhances pair production and changes the spectral distribution of the secondary charged particles. The high atomic number of Gamma Putty also enhances local variation in the angular distribution of secondary electrons, as suggested by several reports [22-23].

In this study, we used an analytical expression to measure electron contamination, and showed that this effect depends on field size and the beam modifier used. Here the source-axis distance (SSD) was set at 100 cm, but some reports [17] have shown that electron contamination is independent of SSD in the range of 100 to 120 cm. In addition, the studies undertaken by Wang *et al.* [24] and Klein *et al.* [25] suggest that the surface dose increases linearly with field size due to electron contamination. Such an outcome is anticipated, since opening the collimators causes more electrons to be generated from the head. We do observe that the contaminant dose at the surface decreased with field size, as demonstrated by Figures 18a and b. The degree of contamination K $(1-v)$ decreases with increasing Gamma Putty thickness for the 6 MV beam. However, K $(1-v)$ does not depend on Gamma Putty thickness for the 18 MV beam, suggesting that the treatment head is the main source of secondary electrons in this case. This study also confirmed that D_{20}/D_{10} increases with field size [Figures 16a and b] and is energy-dependent, but independent of the Gamma Putty thickness.

5. Conclusion

The present work showed how field size, energy, depth, and modifier thickness impact attenuation factors and other dosimetric parameters for photon beams through Gamma Putty modifiers. These models can be used to accurately calculate attenuation factors at any depth, for a wide range of field sizes and Gamma Putty thicknesses. A strong motivation for using analytical models is that they can be used to derive dosimetric parameters for any experimental setup. Such models can also help detect outliers in the data and hence reduce measurement errors. The choice of Gamma Putty as an attenuating material is supported by its general applicability. This study showed that the accurate evaluation of dosimetric parameters for an attenuator does not necessarily require a complete understanding of the spectral distribution. Another advantage of this analytical approach is its ease and accuracy. It eliminates the significant detector-induced systematic measurement uncertainties intrinsic to broad beam geometries.

References

1. El-Khatib E, Podgorsak EB, Pla C. Calculation of dose in homogeneous phantoms for partially attenuated photon beams, *Med. Phys*, 1988; 15(2), 145-50. DOI:10.1118/1.596167
2. Mars JE, Hounsell AR, Wilkinson JM. The efficacy of lead shielding in megavoltage radiotherapy, Br. *J. Radiol*, 1993; 66(782), 140–4. DOI:10.1259/0007-1285-66-782-140
3. Papiez E, Froese G. The calculation of transmission through a photon beam attenuator using sector integration, *Med. Phys*, 1990; 17(2), 281–6. DOI:10.1118/1.596507
4. Castellanos ME, Rosenwald JC. Evaluation of the scatter field for high-energy photon beam attenuators. *Phys. Med. Biol*, 1998; 43(2), 277–90.
5. Tahmasebi Birgani MJ, Karbalaee SM. Calculation of analytical expressions for measured percentage depth dose data in megavoltage photon therapy, *Iranian Red Crescent Medical Journal*, 2009; 11(2), 140-144.
6. Bja¨rngard BE, Tsai JS, Rice RK. Attenuation in very narrow photon beams, *Radiat. Res*, 1989; 118(2), 195–200.
7. Du Plessis, CP, Willemse, CA. Monte Carlo calculation of effective attenuation coefficients for various compensator Materials, *Med Phys*, 2003; 30(9), 2537-44. DOI:10.1118/1.1591432
8. Yang JN, Pino R. Analytical calculation of central-axis dosimetric data for a dedicated 6 MV radiosurgery linear accelerator, *Med Phys*, 2008; 35(10), 4333-41. DOI:10.1118/1.2975142
9. LeBron S, Bo L, Barraclough B, Chiray L. Parameterization of photon beam dosimetry for

linear accelerator, *Med Phys*, 2016; 43(2), 748-60 DOI: 10.1118/1.4939261
10. Bjärngard BE, Shackford H. Attenuation in high-energy x-ray beams, *Med Phys*, 1994; 21(7), 1069-73.
11. Christoph Kleinschmidt. Analytical considerations of beam hardening in medical accelerator photon spectra, *Med Phys*, 1999; 26(9), 1995-99 DOI: 10.1118/1.598704
12. Alles J, Mudde RF. Beam hardening: Analytical considerations of the effective attenuation coefficient of x-ray Tomography, *Med Phys*, 2007; 34(7), 2882-9. DOI:10.1118/1.2742501
13. Leung PM, Sontag MR, Maharah J, Chenersy. Dose measurements in the buildup region for Cobalt 60 therapy units, *Med Phys*, 1976; 3(3), 169-72. DOI:10.1118/1.594220
14. Brahme A, Andreo P. Dosimetry and quality specification of high energy photon beams, *Acta. Radiol. Oncol*, 1986; 25(3), 213-223.
15. Weeks KJ, Fraass BA, Hutchins KM. Gypsum mixtures for compensator construction, *Med Phys*, 1988; 15(3), 410-14. DOI: 10.1118/1.596240
16. Zhu TC, Palta JR. Electron contamination in 8 and 18 MV photon beams, *Med Phys*, 1988; 25(1), 12-9. DOI:10.1118/1.598169
17. Medina LA, Teijeiro A, Garcia J, Esperon J. Characterization of electron contamination in megavoltage photon beams, *Med Phys*, 2005; 32(5), 1281-92. DOI:10.1118/1.1895793
18. Otto A. Sauer and J. Wilbert. Functional representation of tissue phantom ratios for photon fields, *Med Phys*, 2009; 36(12), 5444-50. DOI:10.1118/1.3250867
19. Brahme A, Svensson H. Radiation beam characteristics of a 22 MeV microtron, *Acta Radiol. Oncol Radiat Phys Biol*, 1979; 18, 244–72. DOI: 10.3109/02841867909128212
20. Zhu TC, Das IJ, Bja¨rngard BE. Characteristics of bremsstrahlung in electron beams, *Med Phys*, 2001; 28(7), 1352-8. DOI:10.1118/1.1382608
21. Xiao Y, Altschuler MD, Bjarngard BE. Quality assurance of central axis dose data for photon beams by means of a functional representation of the tissue phantom ratio, *Phys. Med. Biol*, 1998; 43(8), 2195–206.
22. Werner BL, Das IJ, Khan FM, Meigooni AS. Dose perturbations at interfaces in photon beams, *Med. Phys*, 1987; 14(4), 585–95. DOI:10.1118/1.596500
23. Werner BL, Das IJ, Salk WN. Dose perturbations at interfaces in photon beams: secondary electron transport, *Med. Phys*, 1990; 17(2), 212–26. DOI:10.1118/1.596500
24. Wang Y, Khan MK, Ting JY, Easterling SB. Surface dose investigation of the flattening filter-free photon beams, *Int. J. Radiat. Oncol. Biol. Phys*, 2012; 83(2), 281–85. DOI:10.1016/j.ijrobp.2011.12.064
25. Klein EE, Esthappan J, Li Z. Surface and buildup dose characteristics for 6, 10, and 18 MV photons from an Elekta Precise linear accelerator, *J Appl Clin Med Phys*, 2003; 4(1), 1-7. DOI:10.1120/1.1520113

